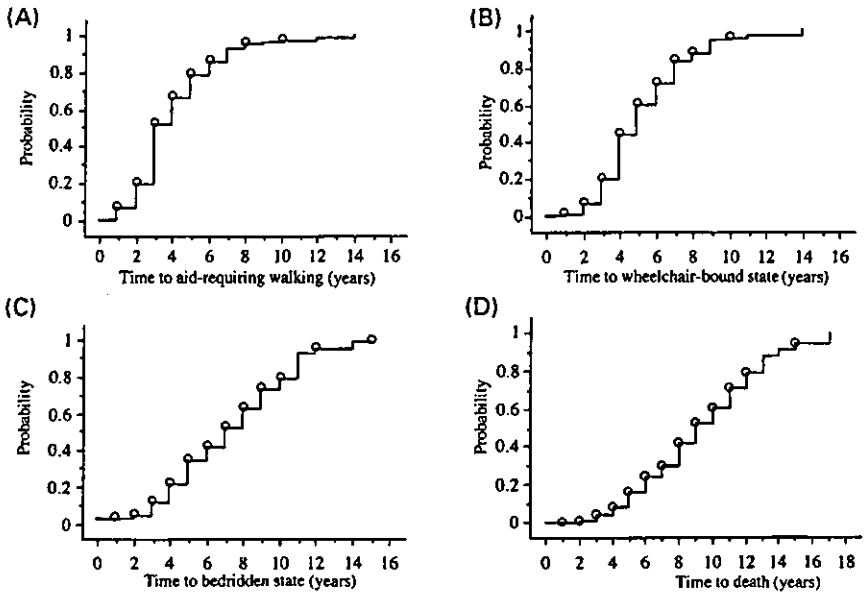

Fig. 3 Activities of daily living (ADL) as milestones indicating disease progression [aid-requiring walking (A), wheelchair-bound state (B), bedridden state (C)] as well as survival in patients (D) with MSA. Kaplan–Meier curves are shown.

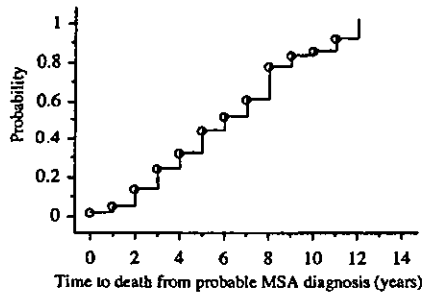

Fig. 4 Estimated time to death from the point of diagnosis of probable MSA. Kaplan–Meier curve.

105 of these patients, and parkinsonism in 61. Sixty-four patients showed autonomic failure as an initial symptom, with urinary symptoms in 44 and postural hypotension in 20. In the MSA-C group, 106 and 49 patients showed cerebellar dysfunction and autonomic failure as initial symptoms, respectively. In the MSA-P group, 60 and 15 patients noted parkinsonism and autonomic failure as initial symptoms, respectively. At diagnosis of MSA, bladder disturbance was evident in 187 patients (82.2%), and postural faintness, blurred vision or syncope was present in 69 (30.0%). Motor impairment versus autonomic failure as the initial symptom did not differ significantly between MSA-C and MSA-P.

Time from onset to evolution to MSA

A Kaplan–Meier estimated time curve from the initial onset to the presence of concomitant motor and autonomic manifestations (evolution from onset to clinical MSA) is presented in Fig. 2. In all MSA patients (Fig. 2A), the median period was 2.0 years (range 1–10 years) while frequency of concomitant manifestations at 2, 4 and 6 years was 57.4, 83.5 and 96.5%, respectively. No significant difference for this interval was noted by a log-rank test comparing MSA-C with MSA-P (Fig. 2B).

Progression, outcome and risk factors

Seventy-eight patients had died at the time of data collection. In 22 of these patients (13 MSA-C, nine MSA-P), autopsy was performed and the diagnosis of definite MSA confirmed. Pathological findings included neuronal loss and astrogliosis in the olivopontocerebellar, striatonigral and autonomic systems as well as corticospinal tracts. Glial cytoplasmic inclusions, a specific hallmark of MSA, were abundant in oligodendroglia as assessed by Gallyas–Braak staining. Figure 3 shows Kaplan–Meier estimates for ADL milestones including aid-requiring walking, wheelchair-bound state, bedridden state and death. These intervals were measured from the time of initial symptom onset. Tracheostomy was performed in 40 patients (23 MSA-C, 17 MSA-P) at 6.3 ± 3.0 years from onset; these patients were treated as censored data from the time of that operation. The median interval from

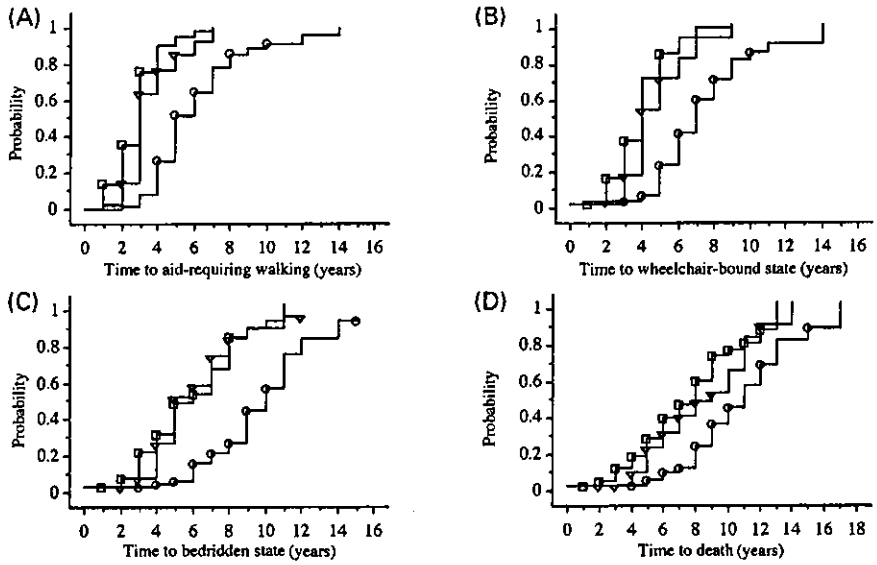

Fig. 5 Kaplan–Meier estimates and the log-rank test were used to compare survival as well as the occurrence of three milestones concerning activities of daily living (ADL) between three groups defined by interval from onset to evolution of concomitant motor and autonomic impairment. Squares, triangles and circles represent censored data, indicating subjects with evolution within 1 year, 2–3 years or after 3 years, respectively. Risk of progression to each ADL milestone or dying differed significantly between evolution rates: (**A**) aid-requiring walking, $P < 0.01$; (**B**) wheelchair dependence, $P < 0.01$; (**C**) bedridden state, $P < 0.01$; and (**D**) death, $P < 0.01$.

Table 2 *Potential risk factors concerning progression and survival*

	Aid-requiring walking		Wheelchair dependence		Bedridden state		Death	
	Median time (years)*	*P* value+	Median time (years)	*P* value	Median time (years)	*P* value (years)	Median time	*P* value
Duration								
≤3 years	5.0	<0.01	7.0	<0.01	10.0	<0.01	11.0	<0.01
>3 years	3.0		4.0		6.0		8.0	
Age at onset								
≤55 years	4.0	0.07	5.0	0.05	8.0	0.03	10.0	0.03
>55 years	3.0		4.0		7.0		8.0	
Type								
MSA-C	4.0	0.03	5.0	<0.01	8.0	<0.01	10.0	0.26
MSA-P	3.0		4.0		6.0		8.0	
Initial symptom								
AF/UD	4.0	<0.01	6.0	<0.01	8.0	0.27	9.0	0.92
Motor	3.0		5.0		7.0		9.0	
Gender								
Male	3.0	0.37	5.0	0.23	8.0	0.62	9.0	0.47
Female	3.0		5.0		7.0		9.0	

*Median survival was calculated by Kaplan–Meier estimates. +Log-rank test statistics were used to determine whether Kaplan–Meier transition curves differed among subgroups. AF/UD = autonomic failure/urinary dysfunction.

onset to aid-requiring walking, wheelchair requirement, bedridden state and death was 3, 5, 8 and 9 years, respectively. The frequency of patients with aid-requiring walking, wheelchair requirement and bedridden state within 5 years of initial onset was 78.4, 59.4 and 31.6%, respectively. Survival rates at 5 and 10 years were 83.5 and 39.9%. The

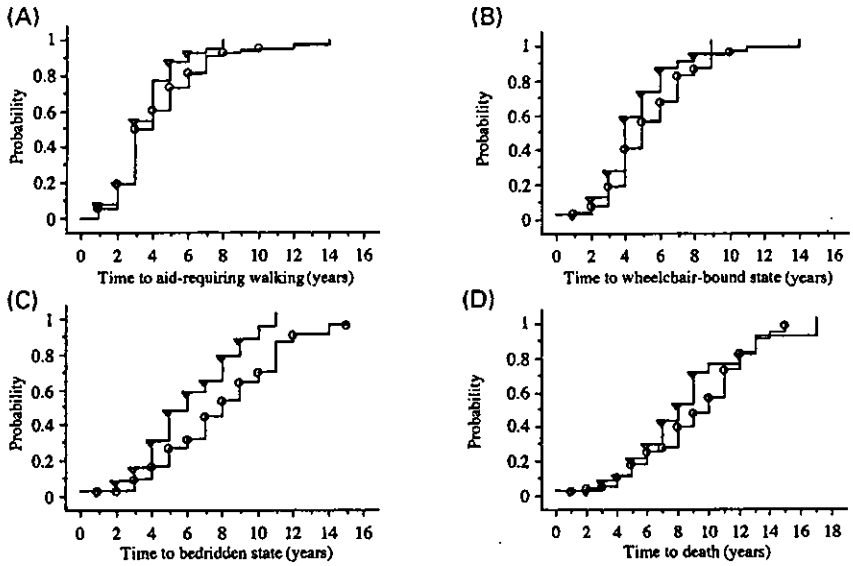

Fig. 6 Difference in time remaining free from three activities of daily living (ADL) milestones as well as survival between MSA-C and MSA-P. Triangles and circles represent censored data, indicating subjects with MSA-P and MSA-C, respectively. Significant differences were seen between the two groups for the three ADL milestones but not for survival by a Kaplan–Meier analysis and the log-rank test: (A) aid-requiring walking, $P = 0.03$; (B) wheelchair dependence, $P < 0.01$; (C) bedridden state, $P < 0.01$; (D) death, $P = 0.26$.

estimated time to death from the point at which patients were diagnosed as probable MSA was 6.0 years, calculated by the Kaplan–Meier method (Fig. 4).

Figure 5 represents the Kaplan–Meier curves of three ADL milestones and of survival estimated in terms of time from initial symptom onset to evolution to MSA including three subgroups: within 1 year, from 1 to 3 years and >3 years. Subgroups representing shorter times from onset to concomitant motor and autonomic system impairment, particularly times not exceeding 3 years, progressed more rapidly to each ADL milestone and to death. These differences were significant by a log-rank test for comparison between evolution-defined subgroups ($P < 0.01$). These results indicate that the shorter the time from onset to evolution to MSA phenotype, the more rapid the progression in ADL milestones and eventual death.

Risk factors evaluated concerning progression and survival are summarized in Table 2. Time from onset to evolution to MSA, age of onset, disease phenotype (MSA-C versus MSA-P) and initial symptom (autonomic versus motor) influenced either progression to ADL milestones or survival to some degree. Patients with concomitant motor and autonomic involvement (evolution time to MSA) within 3 years of onset had a significantly greater risk of entering an advanced disease stage as well as poorer survival than those with a more gradual evolution to MSA. Onset in older individuals also increased the risk of ADL functional deterioration and death. In contrast, MSA-P patients had more rapid functional deterioration than MSA-C patients, but showed similar survival (Fig. 6). Patients whose symptoms of motor impairment preceded autonomic failure had an accelerated risk of requiring walking aid and a wheelchair, but the time until confinement to bedridden state and the survival was no worse. Gender was not predictive of either progression to a more advanced ADL milestone or survival.

Evaluation of MRI abnormalities

Patients who underwent MRI evaluation included 85 with MSA-C and 54 with MSA-P. Neither interval from onset to MRI examination nor gender differed significantly between MSA-C and MSA-P (Table 3).

A hyperintense rim at the lateral edge of the dorsolateral putamen was evident in 31 (32.2%) of 96 patients with MSA on 1.5 T images and 17 (39.5%) of 43 on 0.5 T images. The 'hot cross bun' sign was seen in the pons in 62 (64.5%) of 96 patients on 1.5 T scans and 26 (60.4%) of 43 on 0.5 T scans. Thus the frequency of signal abnormalities was not significantly different between 1.5 T and 0.5 T. With regard to clinical phenotype, the frequency of putaminal abnormality in MSA-P was higher than in MSA-C, and the frequency of pontine abnormality in MSA-C was higher than in MSA-P. MRI signal abnormalities became more frequent with increasing disease duration from onset of the initial symptom and from onset of motor impairment (Table 4).

Table 3 *MRI abnormalities and disease duration from onset to autonomic or motor impairment*

	MSA	MSA-C	MSA-P
1.5 T			
Duration (years)	3.9 ± 2.3	3.8 ± 2.3	4.2 ± 2.4
n (male : female)	96 (54 : 42)	59 (34 : 25)	37 (20 : 17)
MRI findings			
Pontine abnormality *n* (%)	62 (64.5)	48 (81.4)	14 (37.8)
Putaminal abnormality *n* (%)	31 (32.2)	10 (16.9)	21 (56.8)
0.5 T			
Duration (years)	4.3 ± 2.3	4.2 ± 2.5	4.6 ± 2.2
n (male : female)	43 (24 : 19)	26 (14 : 12)	17 (10 : 7)
MRI findings			
Pontine abnormality *n* (%)	26 (60.4)	20 (76.9)	6 (35.3)
Putaminal abnormality *n* (%)	17 (39.5)	6 (23.1)	11 (64.7)

The frequency of pontine signal abnormalities in MSA-C was higher than that of putaminal signal abnormalities in MSA-P.

Table 4 *Symptom duration and frequency of MRI signal abnormality*

	Frequency of pontine abnormality in MSA-C (%)		Frequency of putaminal abnormality in MSA-P (%)	
	Time from onset	Time from motor impairment	Time from onset	Time from motor impairment
≤2 years	78.9	64.0	38.1	38.5
≤4 years	76.2	87.5	65.0	72.2
>4 years	92.9	100	76.9	80.0

Morphometric MRI analysis revealed significant decreases in ratios of CV/MPF, PB/MPF and CC/MISS in patients with MSA compared with control subjects ($P < 0.01$), and the CV/MPF and PB/MPF ratio in patients with MSA-C was significantly smaller than in patients with MSA-P ($P < 0.01$; Fig. 7). The CC/MISS ratio was not significantly different between MSA-C and MSA-P. Both CV/MPF and PB/MPF ratios showed significant negative correlations with disease duration from onset ($r = 0.39$, $P < 0.01$ and $r = 0.44$, $P < 0.01$, respectively; Fig. 8A and B), while the CC/MISS ratio did not show a correlation with duration from onset ($r = 0.10$, $P > 0.5$; Fig. 8C). In patients with MSA-C, a more significant negative correlation was seen between disease duration from onset of cerebellar signs and CV/MPF ($r = 0.71$, $P < 0.01$; Fig. 8D) and PB/MPF ($r = 0.76$, $P < 0.01$; Fig. 8E). When progression of atrophy was assessed on the individual patients, a decrease in CV/MPF, PB/MPF was associated with both disease duration and ADL milestone progression but was highly variable for each ADL milestone between individual patients (Fig. 9).

Discussion

In this study, the calculated median time from onset to evolution to MSA was 2.0 years. Within 4 years, 85% of patients showed both autonomic failure and motor impairment. Median survival time was 9.0 years and ranged from 2 to 17 years, in good agreement with previous studies (Wenning *et al.*, 1994; Klockgether *et al.*, 1998). Our study further documented that rate of progression to multiple system involvement varied among patients but was independent of age of onset, clinical phenotype, initial symptom and gender. Median times from onset to aid-requiring walking, wheelchair requirement and a bedridden state were 3.0, 5.0 and 8.0 years, respectively, as calculated by Kaplan–Meier analysis.

Various factors have been proposed to predict survival in MSA, including gender, age of onset and clinical phenotype (Saito *et al.*, 1994; Schulz *et al.*, 1994; Wenning *et al.*, 1994; Testa *et al.*, 1996; Ben-Shlomo *et al.*, 1997; Klockgether *et al.*, 1998); however, disagreements were evident between these reports. In this study, gender was not associated with worsening of ADL milestones or survival. Wenning *et al.* (1994) previously indicated that gender influenced survival time when early manifestation of sexual dysfunction in men was included as one of the initial symptoms, but gender had no influence when only motor symptoms were considered as an initial symptom. The absence of a gender effect in our results could have been due to excluding sexual dysfunction as an initial symptom. Whether the phenotypes of MSA-P and MSA-C differentially affect survival is controversial (Saito *et al.*, 1994; Schulz *et al.*, 1994; Wenning *et al.*, 1994; Testa *et al.*, 1996; Ben-Shlomo *et al.*, 1997). We found that MSA-P patients had accelerated deterioration with respect to ADL

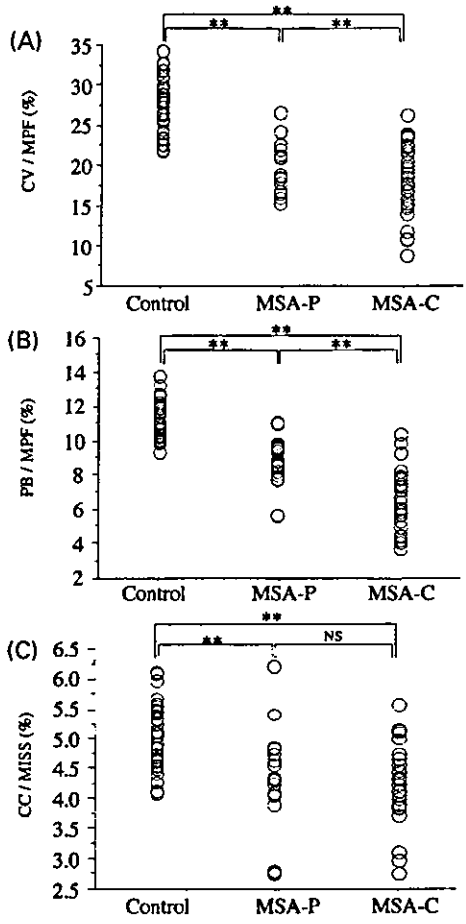

Fig. 7 Relationship between size ratios of brain regions to skull regions (A) CV/MPF; (B) PB/MPF; and (C) CC/MISS (inner table, foramen magnum, clivus, sellar diaphragm, jugum sphenoidale) in patients and control subjects. CV/MPF, PB/MPF and CC/MISS in MSA patients were significantly smaller than in control subjects. The CV/MPF and PB/MPF ratios in MSA-C were much smaller than in MSA-P. The CC/MISS ratio did not differ between MSA-C and MSA-P. $^{**}P < 0.01$ by Mann–Whitney *U* test. NS = not significant.

milestones compared with MSA-C, while survival was no worse. Our results may suggest that parkinsonism affects motor aspects of ADL more profoundly than cerebellar dysfunction. In contrast to gender and clinical phenotype, higher age at onset increased risk of death, in agreement with most previous reports (Wenning *et al.*, 1994; Ben-Shlomo *et al.*, 1997).

A striking observation in our study was that a shorter time of evolution to MSA predicted worse deterioration of ADL and shorter survival. In particular, evolution to MSA within 3 years from onset strongly predicted an aggressive course. Gilman *et al.* (2000) reported that the median life expectancy from symptom onset was 20.7 years in a group with pure cerebellar ataxia, but only 7.7 years in a group with cerebellar ataxia plus non-cerebellar symptoms, particularly parkinsonism; thus the appearance of non-cerebellar symptoms carried a poor prognosis for survival in cerebellar ataxia. This group with pure cerebellar ataxia plus non-cerebellar symptoms was considered to represent MSA (Gilman *et al.*, 2000). Our study indicated that time from initial symptom to appearance of other symptoms indicating evolution to MSA was strongly related to deterioration of ADL and worsening of survival. Although our observation is somewhat similar to that of Gilman *et al.*, in that evolution from single-system impairment to impairment of multiple systems affects survival, our study indicated that early evolution is particularly important for predicting ADL deterioration and poor survival. Why some patients show early evolution to MSA while others show a long interval of restricted system impairment is not known. One possible explanation involves differences in genetic background. Recent studies suggest that widespread accumulation of α-synuclein plays an important role in the pathogenesis of MSA, and possibly in evolution of dysfunction to involve multiple systems (Tu *et al.*, 1998; Dickson *et al.*, 1999). However, polymorphism of various genes including the α-synuclein gene showed no evident effect on development of MSA (Morris *et al.*, 2000). Genetic variation of as yet unidentified genes could be related to evolution time, and much further study is needed to solve these issues.

MRI is a useful procedure not only for diagnosis but also for investigating clinical features of MSA (Stern *et al.*, 1989; Savoiardo *et al.*, 1990; Kume *et al.*, 1992; Konagaya *et al.*, 1994; Wakai *et al.*, 1994; Schrag *et al.*, 1998, 2000; Kraft *et al.*, 1999). A hyperintense putaminal rim and a 'hot cross bun' sign on T_2-weighted images are characteristic MRI signs of MSA (Konagaya *et al.*, 1994; Schwarz *et al.*, 1996; Schrag *et al.*, 1998, 2000). The occurrence of signal abnormalities in the putamen and pons was not significantly different between 1.5 T and 0.5 T examinations, in agreement with previous studies (Schrag *et al.*, 1998, 2000). We found a good correlation between prevalence of signal abnormality and disease duration. Both the putaminal and pontine abnormalities on MRI were significantly accentuated as MSA-P and MSA-C features advanced. Thus, these MRI findings were useful markers for assessing the MSA-P and MSA-C pathology, complementing clinical follow-up examination.

The diagnostic utility of signal abnormality in early MSA remains unclear. In particular, the frequency of a putaminal abnormality in MSA-P was lower than that of pontine abnormalities in MSA-C in all stages. Less prevalent putaminal than pontine abnormality in our series may correspond to a smaller proportion of patients with MSA-P than MSA-C or, alternatively, could be due to a putaminal pathological feature. Iron content in the posterolateral part of the putamen has been reported to increase in MSA (Borit *et al.*, 1975; Vymazal *et al.*, 1999). Thus, a hyperintense putaminal rim signal in MSA-P could be masked by hypointensity due to iron accumulation, particularly in some patients with advanced disease. Further prospective

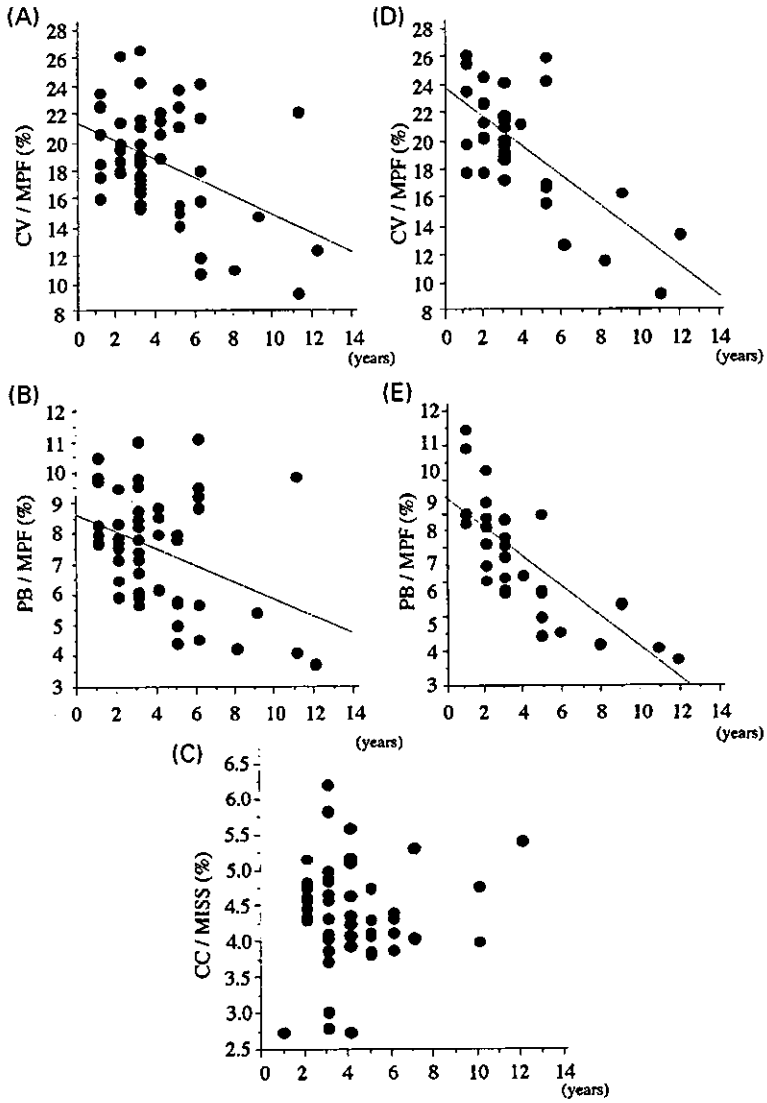

Fig. 8 Relationship between atrophy and disease duration from onset of illness. Significant correlations were seen between duration and both CV/MPF (A) and PB/MPF (B), but not between duration and CC/MISS (C). Relationships between (D) CV/MPF and (E) PB/MPF and disease duration from onset of cerebellar signs in patients with MSA-C showed a more significant negative correlation (CV/MPF, $r = 0.71$, $P < 0.01$; PB/MPF, $r = 0.76$, $P < 0.01$) than disease duration from onset of other symptoms including autonomic failure.

longitudinal MRI assessments will be needed to solve this problem.

The degree of both CV and PB atrophy in patients with MSA-C was more significant than in patients with MSA-P, as in previous reports (Schulz *et al.*, 1994). Although the degrees of both CV and PB atrophy were markedly related to time from onset, CC/MISS varied considerably between cases and was not related to disease duration. Despite this absence of correlation between degree of callosal atrophy and interval from onset, a subgroup of patients showed significant atrophy of the CC. In patients with apparent CC atrophy, cerebral atrophy was also conspicuous. Cerebral atrophy has been reported in cases of MSA with particularly long follow-up periods (Konagaya *et al.*, 1999; Horimoto *et al.*, 2000). Since glial cytoplasmic inclusions have been observed in the cerebral hemisphere (Papp *et al.*, 1994), cerebral peduncle (Yasui *et al.*, 1999) and CC (Costa

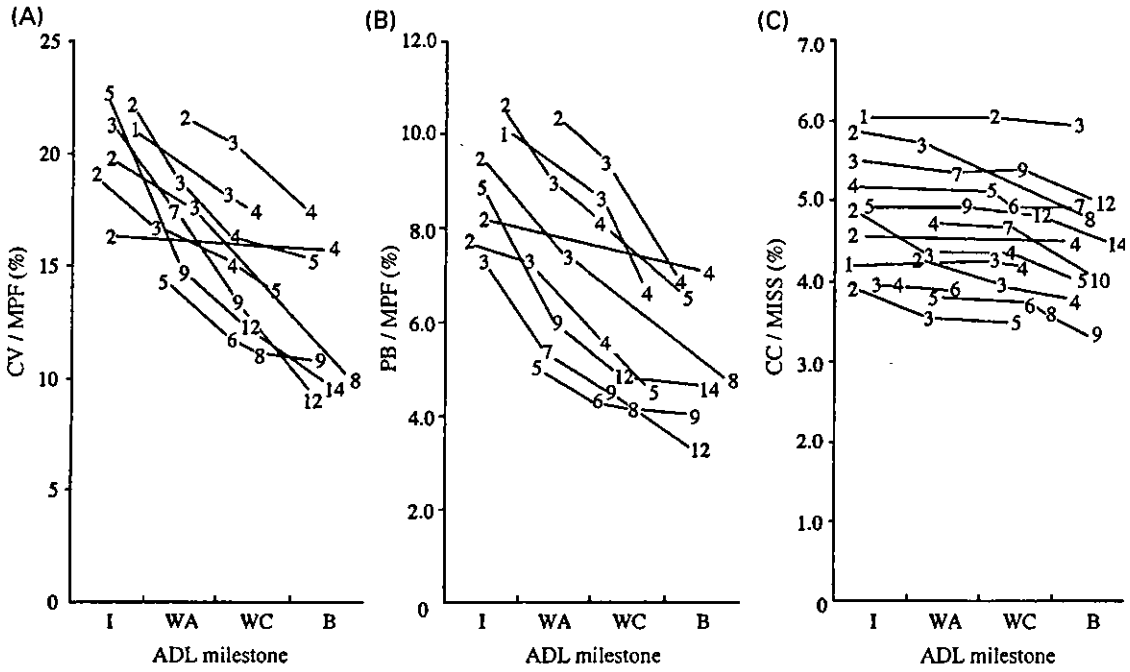

Fig. 9 Longitudinal study of (A) CV/MPF, (B) PB/MPF and (C) CC/MISS ratio in patients with MSA-C. Numbers represent time of MRI as years from disease onset. The CV/MPF, PB/MPF and CC/MISS ratios decreased in association with both disease duration and ADL deterioration. The decrease in CC/MISS in terms of ADL deterioration was less significant as compared with those in CV/MPF and PB/MPF. The CV/MPF, PB/MPF and CC/MISS ratios were variable at each ADL milestone. I = independent gait; WA = aid-requiring walking; WC = wheelchair dependence; B = bedridden state.

et al., 1992), these structures could be expected to atrophy in some MSA patients, as documented in this study. Our result suggests that a subgroup of MSA patients has a tendency toward cerebral hemispheric involvement, even though the cerebellum, pons and putamen are involved more frequently in MSA than the cerebral hemispheres. Evaluation of higher cognitive functions combined with MRI and other neuroimaging procedures in MSA patients should shed light on this problem.

We investigated the correlation between the degree of CV or PB atrophy and interval from clinical onset of evidence of cerebellar dysfunction to MRI, as well as the correlation of such atrophy with ADL deterioration in patients with MSA-C. Decreases in both CV and PB areas correlated strongly with time from onset of cerebellar symptoms, and were related to ADL deterioration to some extent. However, ADL deterioration was highly variable among the individual patients, and both motor ability and functional status did not strictly correspond to the atrophy. Other factors such as the rate of evolution to MSA, age at onset and clinical phenotype could also profoundly influence ADL deterioration, as described in this study.

Wenning *et al.* (1994) reported that MSA-P was the most common manifestation of MSA in a Western population (13.6%), and this finding was supported by some other studies (Testa *et al.*, 1996; Ben-Shlomo *et al.*, 1997). However, the frequency of MSA-C in two reports from Germany (Schulz *et al.*, 1994; Klockgether *et al.*, 1998) was 65.6 and 64.2%, respectively. In the present series, the proportion of MSA-C among Japanese MSA patients was also high (67.4%) and, correspondingly, MSA-P was relatively infrequent (32.6%). Sporadic spinocerebellar degeneration cases predominate over hereditary cases in Japan (2 : 1) (Kita, 1993), in contrast to the findings in Western studies (sporadic : hereditary, 1 : 3) (Polo *et al.*, 1991). In Japan, the percentage of OPCA patients among all spinocerebellar ataxia patients is relatively high (34.4%) (Kita, 1993), although diagnostic criteria used in reports differed from those of Western countries. MSA-C patients in this study had not only late-onset cerebellar ataxia but also additional features, including autonomic failure, fulfilling widely accepted clinical criteria. They did not simply have undifferentiated idiopathic late-onset cerebellar ataxia (Gilman *et al.*, 1996), and did not have features pointing to any other cause. Furthermore, the frequencies of MRI signal

abnormalities in MSA-C were similar to those previously reported (Schrag *et al.*, 1998, 2000), and 13 MSA-C patients examined at autopsy showed typical pathological features. The MSA-C patients in our series thus were considered to have the same clinicopathological nature as those in series from Western countries (Klockgether *et al.*, 1990; Gilman *et al.*, 1996). Although phenotypic differences could be due to physicians' referral patterns, the evidence suggests that the frequency of MSA phenotypes could differ between ethnic populations. Clinico-epidemiological and correlative data comparing MSA between Japanese and Caucasian populations currently are incomplete, but an analysis of ethnic background should be very informative concerning clinical phenotype, disease progression and prognosis of MSA. Factors determining clinical phenotype and evolution of system involvement in MSA are not clear at present, but genetic factors need further exploration.

Acknowledgements

We wish to thank Dr Terunori Mitsuma, Division of Neurology, Fourth Department of Internal Medicine, Aichi Medical University, Japan; Drs Tsutomu Yanagi, Shigetaka Hakusui and Keizo Yasui, Department of Neurology, Nagoya Daini Red Cross Hospital, Japan; Dr Takako Yamada, Department of Neurology, Chubu National Hospital, Japan; and Dr Akiko Yamaoka, Department of Neurology, Higashi Nagoya National Hospital, Japan, for valuable advice and kind suggestions. This work was supported by a COE grant from the Ministry of Education, Culture, Sports, Science and Technology of Japan, and grants from the Ministry of Health, Labour and Welfare of Japan.

References

Abe Y, Tanaka F, Matsumoto M, Doyu M, Hirayama M, Kachi T, et al. CAG repeat number correlates with the rate of brainstem and cerebellar atrophy in Machado–Joseph disease. Neurology 1998; 51: 882–4.

Adams RD, van Bogaert L, van der Eecken H. Dégénérescences nigro-striées et cérébello-nigro-striées (Unicité clinique et variabilité pathologique des dégénérescences préséniles à forme de rigidité extrapyramidale). Psychiat Neurol Basel 1961; 142: 219–59.

Adams RD, van Bogaert L, van der Eecken H. Striato-nigral degeneration. J Neuropathol Exp Neurolol 1964; 23: 584–608.

Bannister R, Oppenheimer DR. Degenerative disease of the nervous system associated with autonomic failure. Brain 1972; 95: 457–74.

Ben-Shlomo Y, Wenning GK, Tison F, Quinn NP. Survival of patients with pathologically proven multiple system atrophy: a meta-analysis. Neurology 1997; 48: 384–93.

Borit A, Rubinstein LJ, Urich H. The striatonigral degenerations: putaminal pigments and nosology. Brain 1975; 98: 101–12.

Costa C, Duyckaerts C, Cervera P, Hauw JJ. Oligodendroglial inclusions, a marker of multisystemic atrophies. [Review]. [French]. Rev Neurol (Paris) 1992; 148: 274–80.

Déjerine J, Thomas AA. L'atrophie olivo-ponto-cérébelleuse. Nouv Iconogr Salpêtr 1900; 13: 330–70.

Dickson DW, Liu W, Hardy J, Farrer M, Mehta N, Uitti R, et al. Widespread alterations of alpha-synuclein in multiple system atrophy. Am J Pathol 1999; 155: 1241–51.

Gilman S, Quinn NP. The relationship of multiple system atrophy to sporadic olivopontocerebellar atrophy and other forms of idiopathic late-onset cerebellar atrophy. [Review]. Neurology 1996; 46: 1197–99.

Gilman S, Low PA, Quinn N, Albanese A, Ben-Shlomo Y, Fowler CJ, et al. Consensus statement on the diagnosis of multiple system atrophy. [Review]. J Neurol Sci 1999; 163: 94–8.

Gilman S, Little R, Johanns J, Heumann M, Kluin KJ, Junck L, et al. Evolution of sporadic olivopontocerebellar atrophy into multiple system atrophy. Neurology 2000; 55: 527–32.

Gosset A, Pellissier JF, Delpuech F, Khalil R. Striatonigral degeneration associated with olivopontocerebellar atrophy. Anatomo-clinical study of 3 cases. [French]. Rev Neurol (Paris) 1983; 139: 125–39.

Graham JG, Oppenheimer DR. Orthostatic hypotension and nicotine sensitivity in a case of multiple system atrophy. J Neurol Neurosurg Psychiatry 1969; 32: 28–34.

Horimoto Y, Aiba I, Yasuda T, Ohkawa Y, Katayama T, Yokokawa Y, et al. Cerebral atrophy in multiple system atrophy by MRI. J Neurol Sci 2000; 173: 109–12.

Johnson RH, Lee GJ, Oppenheimer DR, Spalding JM. Autonomic failure with orthostatic hypotension due to intermediolateral column degeneration. A report of two cases with autopsies. Q J Med 1966; 35: 276–92.

Kita K. Spinocerebellar degeneration in Japan—the features from an epidemiological study. [Japanese]. Rinsho Shinkeigaku 1993; 33: 1279–84.

Klockgether T, Schroth G, Diener HC, Dichgans J. Idiopathic cerebellar ataxia of late onset: natural history and MRI morphology. J Neurol Neurosurg Psychiatry 1990; 53: 297–305.

Klockgether T, Lüdtke R, Kramer M, Abele M, Burk K, Schols L, et al. The natural history of degenerative ataxia: a retrospective study in 466 patients. Brain 1998; 121: 589–600.

Konagaya M, Konagaya Y, Iida M. Clinical and magnetic resonance imaging study of extrapyramidal symptoms in multiple system atrophy. J Neurol Neurosurg Psychiatry 1994; 57: 1528–31.

Konagaya M, Sakai M, Matsuoka Y, Konagaya Y, Hashizume Y. Multiple system atrophy with remarkable frontal lobe atrophy. Acta Neuropathol (Berl) 1999; 97: 423–8.

Kraft E, Schwarz J, Trenkwalder C, Vogl T, Pfluger T, Oertel WH. The combination of hypointense and hyperintense signal changes on T2-weighted magnetic resonance imaging sequences. A specific marker of multiple system atrophy? Arch Neurol 1999; 56: 225–8.

Kume A, Takahashi A, Hashizume Y, Asal J. A histometrical

and comparative study on Purkinje cell loss and olivary nucleus cell loss in multiple system atrophy. J Neurol Sci 1991; 101: 178–86.

Kume A, Shiratori M, Takahashi A, Kato T, Ito K, Tadokoro M, et al. Hemi-parkinsonism in multiple system atrophy: a PET and MRI study. J Neurol Sci 1992; 110: 37–45.

Kume A, Takahashi A, Hashizume Y. Neuronal cell loss of the striatonigral system in multiple system atrophy. J Neurol Sci 1993; 117: 33–40.

Laissy JP, Patrux B, Duchateau C, Hannequin D, Hugonet P, Ait-Yahia G, et al. Midsaggital MR measurements of the corpus callosum in healthy subjects and diseased patients: a prospective survey. Am J Neuroradiol 1993; 14: 145–54.

Litvan I, Goetz CG, Jankovic J, Wenning GK, Booth V, Bartko JJ, et al. What is the accuracy of the clinical diagnosis of multiple system atrophy? Arch Neurol 1997; 54: 937–44.

Lowe J, Lennox G, Leigh PN. Disorders of movement and system degenerations. In: Graham DI, Lantos PL, editors. Greenfield's neuropathology, Vol. 2. 6th edn. London: Arnold; 1997. p. 281–366.

Mathias CJ, Bannister R. Investigation of autonomic disorders. In: Mathias CJ, Bannister R, editors. Autonomic failure: a textbook of clinical disorders of the autonomic nervous system. 4th edn. Oxford: Oxford University Press; 1999. p. 169–95.

Morris HR, Vaughan JR, Datta SR, Bandopadhyay R, Rohan De Silva HA, Schrag A, et al. Multiple system atrophy/progressive supranuclear palsy: α-synuclein, synphilin, tau, and APOE. Neurology 2000; 55: 1918–20.

Nakazato Y, Yamazaki H, Hirato J, Ishida Y, Yamaguchi H. Oligodendroglial microtubular tangles in olivopontocerebellar atrophy. J Neuropathol Exp Neurol 1990; 49: 521–30.

Papp MI, Lantos PL. The distribution of oligodendroglial inclusions in multiple system atrophy and its relevance to clinical symptomatology. Brain 1994; 117: 235–43.

Papp MI, Kahn JE, Lantos PL. Glial cytoplasmic inclusions in the CNS of patients with multiple system atrophy (striatonigral degeneration, olivopontocerebellar atrophy and Shy–Drager syndrome). J Neurol Sci 1989; 94: 79–100.

Peto R, Pike MC, Armitage P, Breslow NE, Cox DR, Howard SV, et al. Design and analysis of randomized clinical trials requiring prolonged observation of each patient. II. Analysis and examples. Br J Cancer 1977; 35: 1–39.

Polinsky RJ. Multiple system atrophy. Clinical aspects, pathophysiology, and treatment. Neurol Clin 1984; 2: 487–98.

Polo JM, Calleja J, Combarros O, Berciano J. Hereditary ataxias and paraplegias in Cantabria, Spain. Brain 1991; 114: 855–66.

Riku S, Hashizume Y. A clinico-pathological study on multiple system atrophy, with special reference to its striato-nigral lesions and motor neuron involvements. [Japanese]. Rinsho Shinkeigaku 1984; 24: 552–61.

Saito Y, Matsuoka Y, Takahashi A, Ohno Y. Survival of patients with multiple system atrophy. Intern Med 1994; 33: 321–5.

Savoiardo M, Strada L, Girotti F, Zimmerman RA, Grisoli M, Testa D, et al. Olivopontocerebellar atrophy: MR diagnosis and relationship to multiple system atrophy. Radiology 1990; 174: 693–6.

Schrag A, Kingsley D, Phatouros C, Mathias CJ, Lees AJ, Daniel SE, et al. Clinical usefulness of magnetic resonance imaging in multisystem atrophy. J Neurol Neurosurg Psychiatry 1998; 65: 65–71.

Schrag A, Good CD, Miszkiel K, Morris HR, Mathias CJ, Lees AJ, et al. Differentiation of atypical parkinsonian syndromes with routine MRI. Neurology 2000; 54: 697–702.

Schulz JB, Klockgether T, Petersen D, Jauch M, Muller-Schauenburg W, Spieker S, et al. Multiple system atrophy: natural history, MRI morphology, and dopamine receptor imaging with 123IBZM-SPECT. J Neurol Neurosurg Psychiatry 1994; 57: 1047–56.

Schwarz J, Weis S, Kraft E, Tatsch K, Bandmann O, Mehraein P, et al. Signal changes on MRI and increases in reactive microgliosis, astrogliosis, and iron in the putamen of two patients with multiple system atrophy. J Neurol Neurosurg Psychiatry 1996; 60: 98–101.

Shy GM, Drager GA. A neurological syndrome associated with orthostatic hypotension: a clinical–pathologic study. Arch Neurol 1960; 2: 511–27.

Sobue G, Hashizume Y, Ohya M, Takahashi A. Shy–Drager syndrome: neuronal loss depends on size, function, and topography in ventral spinal outflow. Neurology 1986; 36: 404–7.

Sobue G, Hashizume Y, Mitsuma T, Takahashi A. Size-dependent myelinated fiber loss in the corticospinal tract in Shy–Drager syndrome and amyotrophic lateral sclerosis. Neurology 1987; 37: 529–32.

Sobue G, Terao S, Kachi T, Ken E, Hashizume Y, Mitsuma T, et al. Somatic motor efferents in multiple system atrophy with autonomic failure: a clinico-pathological study. J Neurol Sci 1992; 112: 113–25.

Spokes EG, Bannister R, Oppenheimer DR. Multiple system atrophy with autonomic failure. J Neurol Sci 1979; 43: 59–82.

Stern MB, Braffman BH, Skolnick BE, Hurtig HI, Grossman RI. Magnetic resonance imaging in Parkinson's disease and parkinsonian syndrome. Neurology 1989; 39: 1524–6.

Takahashi A, Takagi S, Yamamoto K, Yamada T, Ando K. Shy–Drager syndrome. Its correlation with olivo-ponto-cerebellar atrophy. Rinsho Shinkeigaku 1969; 9: 121–9.

Terao S, Sobue G, Hashizume Y, Mitsuma T, Takahashi A. Disease-specific patterns of neuronal loss in the spinal ventral horn in amyotrophic lateral sclerosis, multiple system atrophy and X-linked recessive bulbospinal neuronopathy, with special reference to the loss of small neurons in the intermediate zone. J Neurol 1994; 241: 196–203.

Testa D, Filippini G, Farinotti M, Palazzini E, Caraceni T. Survival in multiple system atrophy: a study of prognostic factors in 59 cases. J Neurol 1996; 243: 401–4.

Tu PH, Galvin JE, Baba M, Giasson B, Tomita T, Leight S, et al. Glial cytoplasmic inclusions in white matter oligodendrocytes of multiple system atrophy brains contain insoluble alpha-synuclein. Ann Neurol 1998; 44: 415–22.

Vymazal J, Righini A, Brooks RA, Canesi M, Mariani C, Leonardi M, et al. T1 and T2 in the brain of healthy subjects, patients with Parkinson disease, and patients with multiple system atrophy: relation to iron content. Radiology 1999; 211: 489–95.

Yasui K, Hashizume Y, Yoshida M, Sobue G. The cerebral peduncle lesion in multiple system atrophy. [Japanese]. Rinsho Shinkeigaku 1999; 39: 1125–31.

Wakai M, Kume A, Takahashi A, Ando T, Hashizume Y. A study of parkinsonism in multiple system atrophy: clinical and MRI correlation. Acta Neurol Scand 1994; 90: 225–31.

Wenning GK, Ben-Shlomo Y, Magalhaes M, Daniel SE, Quinn NP. Clinical features and natural history of multiple system atrophy: an analysis of 100 cases. Brain 1994; 117: 835–45.

Wenning GK, Ben-Shlomo Y, Magalhaes M, Daniel SE, Quinn NP. Clinicopathological study of 35 cases of multiple system atrophy. J Neurol Neurosurg Psychiatry 1995; 58: 160–6.

Wenning GK, Tison F, Ben-Shlomo Y, Daniel SE, Quinn NP. Multiple system atrophy: a review of 203 pathologically proven cases. Mov Disord 1997; 12: 133–47.

Received July 23, 2001. Revised December 4, 2001.
Accepted January 7, 2002

Journal of Neurochemistry, 2002, **82**, 576–584

X-Linked inhibitor of apoptosis protein is involved in mutant SOD1-mediated neuronal degeneration

Shinsuke Ishigaki, Yideng Liang, Masahiko Yamamoto, Jun-ichi Niwa, Yoshio Ando, Tsuyoshi Yoshihara, Hideyuki Takeuchi, Manabu Doyu and Gen Sobue

Department of Neurology, Nagoya University Graduate School of Medicine, Nagoya, Japan

Abstract

Mutations in the superoxide dismutase 1 (SOD1) gene cause the degeneration of motor neurons in familial amyotrophic lateral sclerosis (FALS). An apoptotic process including caspase-1 and -3 has been shown to participate in the pathogenesis of FALS transgenic (Tg) mouse model. Here we report that IAP proteins, potent inhibitors of apoptosis, are involved in the FALS Tg mouse pathologic process. The levels of X-linked inhibitor of apoptosis protein (XIAP) mRNA and protein were significantly decreased in the spinal cord of symptomatic G93A-SOD1 Tg mice compared with littermates. In contrast, the levels of cIAP-1 mRNA and protein were increased in symptomatic G93A-SOD1 Tg mice, whereas the levels of cIAP-2 mRNA and protein were unchanged. *In situ* hybridization showed that the expression of XIAP was remarkably reduced in the motor neurons of Tg mice, and the expression of cIAP-1 was strongly increased in the reactive astrocytes of Tg mice. Overexpression of XIAP markedly inhibited the cell death and caspase-3 activity in the neuro2a cells expressing mutant SOD1. Deletional mutant analysis revealed that the N-terminal domain of XIAP, the BIR1-2 domains, was essential for this inhibitory activity. These results suggest that XIAP plays a role in the apoptotic mechanism in the progression of disease in mutant SOD1 Tg mice and holds therapeutic possibilities for FALS.

Keywords: amyotrophic lateral sclerosis, caspase-3, cIAP-1, motor neuron disease, SOD1, X-linked inhibitor of apoptosis protein.

J. Neurochem. (2002) **82**, 576–584.

Amyotrophic lateral sclerosis (ALS) is a late-onset neurodegenerative disorder characterized by selective motor neuron death in the spinal cord, brainstem and cerebral cortex. A variety of mutations in the Cu/Zn superoxide dismutase gene (SOD1) are present in about 20% of patients with familial ALS (FALS) (Rosen *et al.* 1993).

Although the primary pathogenesis of ALS remains unknown, the mechanism of apoptosis is thought to be involved in neuronal cell death in this disorder. The expression level of bcl-2 decreases in the ALS spinal cord, and its overexpression delays the disease onset in mutant SOD1 transgenic (Tg) mice and rescues neurons harboring mutant SOD1 from cell death (Ghadge *et al.* 1997; Kostic *et al.* 1997; Lee *et al.* 2001). Caspase-1 and caspase-3 are activated in mutant SOD1 Tg mice and neuro2a cells expressing mutant SOD1 gene (Passinelli *et al.* 1998; Passinelli *et al.* 2000; Vukosavic *et al.* 2000), and the administration of zVAD-fmk, a broad caspase inhibitor, delays the disease onset and mortality of mutant SOD1 Tg mice (Li *et al.* 2000). Although neither TUNEL staining nor DNA fragmentation has been observed in SOD1 Tg models, such evidence supports the view that the mechanism of apoptosis is involved in the pathogenesis of mutant SOD1-mediated ALS.

The inhibitory apoptosis proteins (IAPs) regulate apoptotic cell death by way of caspase inhibition. The X-linked inhibitors of apoptosis protein (XIAP), cIAP-1 and cIAP-2,

Received April 2, 2002; revised manuscript received April 17, 2002; accepted April 17, 2002.

Address correspondence and reprint requests to: Dr Gen Sobue, Department of Neurology, Nagoya University Graduate School of Medicine, Nagoya 466-8550, Japan. E-mail: sobueg@med.nagoya-u.ac.jp

Abbreviations used: ALS, amyotrophic lateral sclerosis; BIR, baculovirus inhibitory repeat; FALS, familial amyotrophic lateral sclerosis; FAM, 6-carboxyfluorescein; GFAP, glial fibrillary acidic protein; GADPH, glyceraldehyde-3-phosphate dehydrogenase; IAP, inhibitory apoptosis protein; ISH, *in situ* hybridization; LM, littermate; MTT, 3-(4,5-dimethylthiazol-2yl)-2,5-diphenyltetrazolium bromide; PI, propidium iodide; RIPA, ristocetin-induced platelet agglutination; SDS–PAGE, sodium dodecyl sulfate–polyacrylamide gel electrophoresis; SOD1, superoxide dismutase 1; TAMRA, 6-carboxytetramethylrhodamine; Tg, transgenic; WT, wild type; XIAP, X-linked inhibitor of apoptosis protein.

interact with caspases-3, -7 and -9, resulting in a direct inhibition of their activity (Deveraux *et al.* 1997; Roy *et al.* 1997). XIAP is the most potent of the IAP proteins and contains two conserved motifs, the baculovirus inhibitory repeats (BIR) and zinc finger-like RING finger (Deveraux *et al.* 1998). Deletional analysis revealed that the second BIR domain (BIR2) is sufficient for XIAP to suppress the activity of caspase-3 and -7, whereas the third BIR domain (BIR3) and RING finger motif are specific for the inhibition of caspase-9 (Takahashi *et al.* 1998; Deveraux *et al.* 1999). Recent studies indicated that XIAP has ubiquitin-protein ligase activity, which promotes caspase-3 degradation (Yang *et al.* 2000; Suzuki *et al.* 2001a).

In a previous study we identified the differentially expressed genes in G93A-SOD1 Tg mice using a cDNA microarray, which showed that the expression level of XIAP mRNA decreased in the spinal cord of G93A-SOD1 Tg mice (Yoshihara *et al.* 2002). Another recent study demonstrated that the cleavage of XIAP and the activation of caspase-9 occurred in the spinal cord of G93A-SOD1 Tg mice (Guégan *et al.* 2001).

Here we report that the levels of XIAP mRNA and protein are depleted, but the levels of cIAP-1 mRNA and protein are increased in the spinal cord of symptomatic G93A-SOD1 Tg mice, and that the induction of the full length XIAP and the N-terminal fraction, BIR1-2, rescues neuro2a cells harboring mutant SOD1 from death by inhibiting the activation of caspase-3. Our data indicate that XIAP plays a pivotal role in the pathogenesis of ALS with mutant SOD1, and that its gene transduction has the potential to contribute to advances in neuroprotection therapy in the future.

Materials and methods

SOD1 Tg mouse

Tg mice expressing the human SOD1 gene with a G93A mutation (Gurney *et al.* 1994) were purchased from the Jackson Laboratory (Bar Harbor, ME, USA) and maintained as hemizygotes by mating Tg males with B6/SJLF1 females. Non-transgenic littermates (LMs) were used as controls. At 11, 14 and 17 weeks of age, three Tg and LM mice at each of these three ages were killed under deep anesthesia according to the guidelines of the ethical committee of the Animal Experimental Center, Nagoya University School of Medicine. The lumbar spinal cords and the brains (whole cerebrum without motor cortex) were quickly frozen in liquid nitrogen, then stored at − 80°C until use.

Quantitative real-time RT-PCR

Total RNA (5 μg) from the lumbar spinal cord and brain (whole cerebrum without motor cortex) of the G93A-SOD1 Tg and LM mice were reverse transcribed into first-strand cDNA, using 20 U Superscript II (Life Technologies, Grand Island, NY, USA). The probe and primers for the real-time PCR were designed with 'Primer 3' (S Rozen and H J Skaletsky, available at http://www-genome.wi.mit.edu/genome_software/other/primer3.html).

Standard templates were prepared by performing PCR (approximately 500 bp) on the outer region for the TaqMan PCR primers from mouse brain cDNA. Each standard template was purified using a PCR purification kit (Qiagen, Valencia, CA, USA), and then used for construction of a standard curve relating threshold cycle to template weight.

FAM (6-carboxyfluorescein) was used as the reporter, and TAMRA (6-carboxytetramethylrhodamine) as the quencher dye. TaqMan PCR was carried out using an iCycler system (Bio-Rad Laboratories, Hercules, CA, USA) on the cDNA samples; 50 μL with 10X PCR buffer, dNTP mix 200 μM, probe 150 nM, primers 300 nM each, 0.25 U rTaq (all reagents from Takara, Otsu, Japan), and 1 μL cDNA template. The reaction conditions were 95°C for 3 min and then 50 cycles of 15 s at 95°C (denaturation) followed by 60 s at 55°C (annealing and extension). All experiments were carried out in quadruplicate, and several negative controls were included. Fluorescence emission spectra were continuously monitored and analyzed with sequence detection software. For internal standard control, the expression of glyceraldehyde-3-phosphate dehydrogenase (GAPDH) was simultaneously quantified.

Primers and probe sequences (forward primer, reverse primer, and TaqMan probe): [XIAP] 5′-CCATGTGTAGTGAAGAAGCCAGAT-3′, 5′-TGATCATCAGCCCCTGTGTAGTAG-3′, 5′-TCATTTCAGAACTGGCCGGACTATGCTC-3′, [cIAP-1] 5′-CGAGGAGGAGGAGTCAGATG-3′, 5′-GGAGGCAATACAGCATTGGT-3′, 5′-CACTAATCCGGAAGAACAAAATGGTGCTTT-3′, [cIAP-2] 5′-TGGATCGCAATGATGATGTC-3′, 5′-GAAACCATTTGGCGTGTTCT-3′, 5′-CTTTTGTTGTGATGGTGGCTTGAGATGTT-3′, [GAPDH] 5′-CCTGGAGAAACCTGCCAAGTAT-3′, 5′-TGAAGTCGCAGGAGACAACCT-3′, 5′-CATCAAGAAGGTGGTGAAGCAGGCATC-3′.

The threshold cycle of each gene was determined as the number of PCR cycles at which the increase in reporter fluorescence is 10 times above a baseline signal. Log starting quantity gives the weight of the gene contained in each sample. The weight ratio of the target gene to GAPDH gives the standardized expression level.

In situ hybridization and immunohistochemistry

Frozen sections (6-μm thick) of the spinal cord and the brain were prepared and fixed in 4% paraformaldehyde immediately. The deparaffinized sections were treated with proteinase K, refixed in 4% paraformaldehyde, and prepared for *in situ* hybridization (ISH). Digoxigenin-labeled cRNA probes of approximately 500 bp were generated for ISH from linearized plasmids for XIAP and cIAP-1, using Sp6 or T7 polymerase (Boehringer Mannheim, Mannheim, Germany). Control sense probes were also generated from each plasmid using the reciprocal RNA polymerase. This procedure has been described in detail in previous reports (Ishigaki *et al.* 2000; Doyu *et al.* 2001; Niwa *et al.* 2001).

After the ISH procedures, sections of 17-week-old Tg and LM spinal cords were incubated with anti-glial fibrillary acidic protein (GFAP) antibody (Dako, Kyoto, Japan) overnight at 4°C as described previously (Yamamoto *et al.* 2001). The washed sections were incubated with alkaline phosphatase-conjugated anti-rabbit Ig or anti-mouse Ig antibody (Dako). The signal was visualized with Fast Red (Dako).

Western blot

Lumbar spinal cords and brains (whole cerebrum without motor coetex) of 14-week-old SOD1 Tg and LM mice were lysed in ristocetin-induced platelet agglutination (RIPA) buffer. Each protein was separated on 5–20% sodium dodecyl sulfate–polyacrylamide gel electrophoresis (SDS–PAGE) for 45 min (200 V). Five micrograms of protein was used for actin, 10 μg for XIAP, 50 μg for cIAP-1 and cIAP-2. Proteins were transferred to nitrocellulose membranes for 90 min (100 V). The membranes were incubated overnight with anti-actin (Sigma, St Louis, MO, USA), anti-XIAP (Transduction Laboratories, Lexington, KY, USA), anti-cIAP-1 (R & D Systems, Minneapolis, MN, USA), and anti-cIAP-2 (R & D Systems) antibodies, respectively. ECL + Plus (Amersham Pharmacia Biotech, Piscataway, NJ, USA) was used for signal detection.

Vectors

Human G93A and G85R constructs were kindly provided by Dr Naoyuki Taniguchi, Department of Biochemistry, Osaka University Medical School. Human wild-type (WT)-, G93A- and G85R-SOD1- pcDNA3.1/MycHis vectors were prepared by PCR using the primers [SOD1-F] 5′-GTCAGGATCCACCACCATGGCGACGAAGGCCG-3′ and [SOD1-R] 5′-ATATCTCGAGTTGGGCGATCCCAATTACACC-3′. PCR products were inserted into the BamHI-XhoI site in pcDNA3.1/Mic-His A (Invitrogen, Carlsbad, CA, USA). To construct expression clones for mouse XIAP-pcDNA4/His-Max, the coding regions of XIAP were amplified from mouse brain cDNA libraries using primers [XIAP-F] 5′-GTCAGGATCCTATGACTTTTAACAGTT-3′ and [XIAP-R] 5′-ATATCTCGAGCTAAGACATAAAAATTTTTTGGTT-3′. The deletional construct, BIR1-2 (residues 1–241), was generated by the primers [XIAP-F], and [XIAP-MR] 5′-ATATCTCGAGCTAAGATTCACTTCGAACATTAAC-3′. BIR3-RING (residues 242–496) was generated by the primers [XIAP-MF] 5′-GTCAGGATCCTATGGGTGTGAGTTCTG-3′ and [XIAP-R]. PCR products were inserted into the BamHI-XhoI site in pcDNA4/HisMax (Invitrogen). The pcDNA4/HisMax-LacZ (Invitrogen) vector was used as a control vector. The cloned PCR product was sequenced to exclude PCR-generated errors.

Cell viability and cell death assay

Neuro2a cells were maintained and transfected as described previously (Ishigaki *et al.* 2000). Neuro2a cells (5000 cells/well) were grown in 96-well collagen-coated plates overnight. They were then transfected with 0.1 μg of WT-SOD1-pcDNA3.1/MycHis (WT-SOD1), G93A-SOD1-pcDNA3.1/MycHis (G93A-SOD1) or G85R-SOD1-pcDNA3.1/MycHis (G85R-SOD1) and 0.1 μg of XIAP-pcDNA4/HisMax (XIAP), BIR1-2-pcDNA4/HisMax (BIR1-2), BIR3-RING-pcDNA4/HisMax (BIR-RING) or pcDNA4/HisMax-LacZ (LacZ) using Effecten reagent (Qiagen, Valencia, CA, USA). Then 3-(4,5-dimethylthiazol-2yl)-2,5-diphenyltetrazolium bromide (MTT) assays were performed using Cell Titer 96 (Promega, Madison, WI, USA) at 0, 24 and 48 h after incubation. The assays were carried out in triplicate. Absorbance (490 nm) was measured in a multiple plate reader.

For cell death assay, neuro2a cells were grown on two-well collagen-coated slides overnight. Then they were transfected with 0.4 μg of WT, G93A or G85R, 0.4 μg of XIAP, BIR1-2, BIR3-RING or LacZ, and 0.4 μg of C3-EGFP (Clontech, Palo Alto, CA, USA). Cells were incubated for 16 h, and then the medium was changed without serum. Cell mortality was measured by propidium iodide (PI) staining 48 h after serum deprivation. The death cell ratio was calculated as a percentage of PI positive cells among the GFP positive cells.

Caspase-3 activity

Neuro2a cells were transfected with WT-SOD1, G93A-SOD1 or G85R-SOD1 and XIAP or LacZ followed by 48 h of serum deprivation and oxidative stress (4 h of H_2O_2; 100 μM). Cells were lysed in a lysis buffer (50 mM Tris HCl, 150 mM NaCl, 1% Nonidet P-40, 0.1% SDS). Ten micrograms of each protein was analyzed by western blot using anti-caspase-3, H-277 (Santa Cruz Biotechnology, Santa Cruz, CA, USA) antibody.

Results

Quantitative RT-PCR for XIAP, cIAP-1 and cIAP-2 mRNA in spinal cord and brain of G93A-SOD1 Tg mice

Using real-time TaqMan PCR, XIAP, cIAP-1 and cIAP-2 mRNA in the spinal cord of G93A-SOD1 Tg and LM mice were quantified. The expression level of XIAP mRNA in G93A-SOD1 Tg mice had decreased at 14 and 17 weeks as compared with that of LM mice, whereas there was no significant difference at 11 weeks. In contrast, the expression level of cIAP-1 mRNA significantly increased in G93A-SOD1 Tg mice at 14 and 17 weeks. The level of cIAP-2 mRNA did not show any significant difference at any age (Fig. 1a). Neither the expression of XIAP, cIAP-1 nor cIAP-2 mRNA showed any difference in the brain of G93A-SOD1 Tg and LM mice at 14 weeks (Fig. 1b).

Analysis of XIAP, cIAP-1, cIAP-2 proteins in spinal cord and brain of G93A-SOD1 Tg mice

Western blot analysis of the spinal cord showed that the level of XIAP protein was significantly depleted in G93A-SOD1 Tg mice compared with LMs at 14 weeks, whereas the level of cIAP-1 protein increased in G93A-SOD1 Tg mice. The level of cIAP-2 protein was unchanged (Fig. 2a). Western blot using the brain showed that the levels of these IAP family proteins were unchanged between G93A-SOD1 Tg and LM mice at 14 weeks (Fig. 2b).

Tissue distribution of XIAP and cIAP-1 mRNA in spinal cord and brain of G93A-SOD1 Tg mice

For further analysis of the tissue distribution of XIAP and cIAP-1 mRNA in the spinal cord of G93A-SOD1 Tg mice, ISH was performed. The expression of XIAP mRNA was seen in both motor neurons and, to a lesser extent, in glial cells in the spinal cords of LMs. In G93A-SOD1 Tg mice, the hybridization signal of XIAP mRNA was significantly decreased in a subpopulation of motor neurons at 14- and 17-week-old, indicating that the expression levels of XIAP

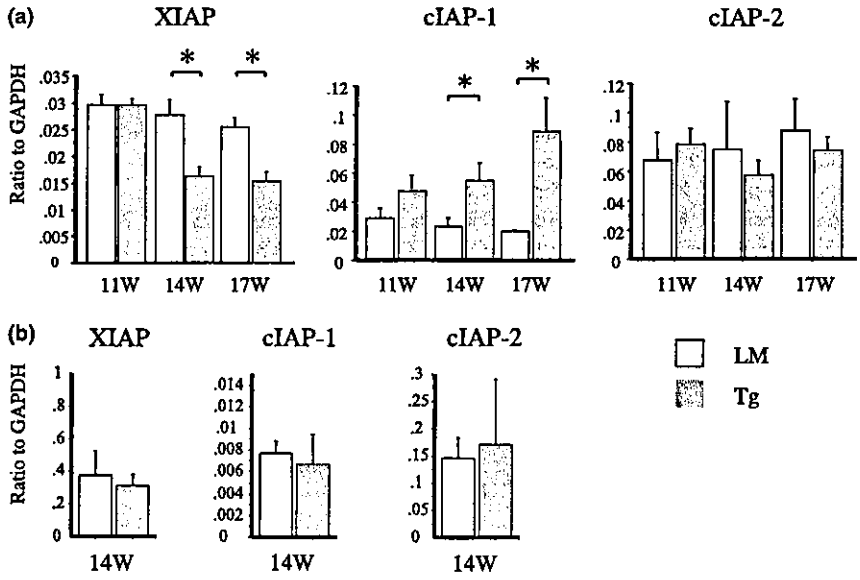

Fig. 1 Quantitative analysis of XIAP, cIAP-1 and cIAP-2 mRNA in the spinal cord (a) and brain (b) of G93A-SOD1 transgenic mice (Tg) and normal littermates (LM) by real-time RT-PCR using TaqMan probes. Quantities are shown as the ratio to GAPDH mRNA. Three mice of each kind were examined at 11, 14 and 17 weeks of age for analysis of the spinal cord, and at 14 weeks for analysis of the brain. Values are the means ± SD, $n = 3$, statistics were carried out by Student's *t*-test, $^*p < 0.05$, significant difference between LM mice and G93A-SOD1 Tg mice.

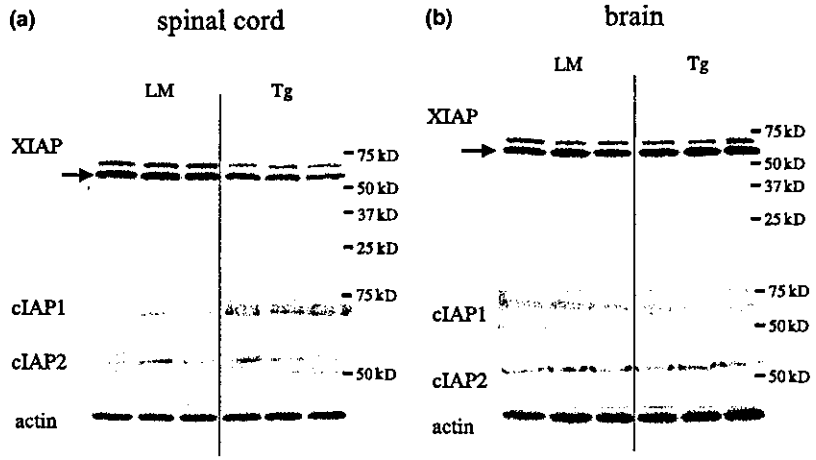

Fig. 2 Protein analysis of XIAP, cIAP-1 and cIAP-2 in the spinal cord and brain of G93A-SOD1 Tg mice. XIAP, cIAP-1 and cIAP-2 protein expressions were analyzed by western blot in the spinal cord (a) and brain (b) from G93A-SOD1 transgenic mice (Tg) ($n = 3$) and normal littermates (LM) ($n = 3$) at the age of 14 weeks. Each lane corresponds to a different animal.

mRNA per individual neurons were diminished in mutant SOD1 Tg mice. The morphological appearance of these neurons with lower XIAP mRNA expression was indistinguishable from that of normal motor neurons (Fig. 3a). The expression of cIAP-1 mRNA was also seen in motor neurons and glial cells, but the signal intensity in the glial cells was weaker than in the motor neurons. However, the expression of cIAP-1 mRNA in the glial cells, especially in astrocytes, markedly increased in mutant SOD1 Tg mice compared with LM mice, particularly at 17 weeks (Figs 3b and c).

The expression of XIAP and cIAP-1 mRNA in the brain was observed mainly in hippocampus neurons, and there was no difference in their expression levels between G93A-SOD1 Tg and LM mice at 14 weeks (Fig. 3d).

Overexpression of XIAP protects against cell death in neuro2a cells expressing mutant SOD1

The MTT assay was performed at 0, 24 and 48 h of incubation. At zero time there was no significant difference in viability between cells with WT-SOD1 and LacZ

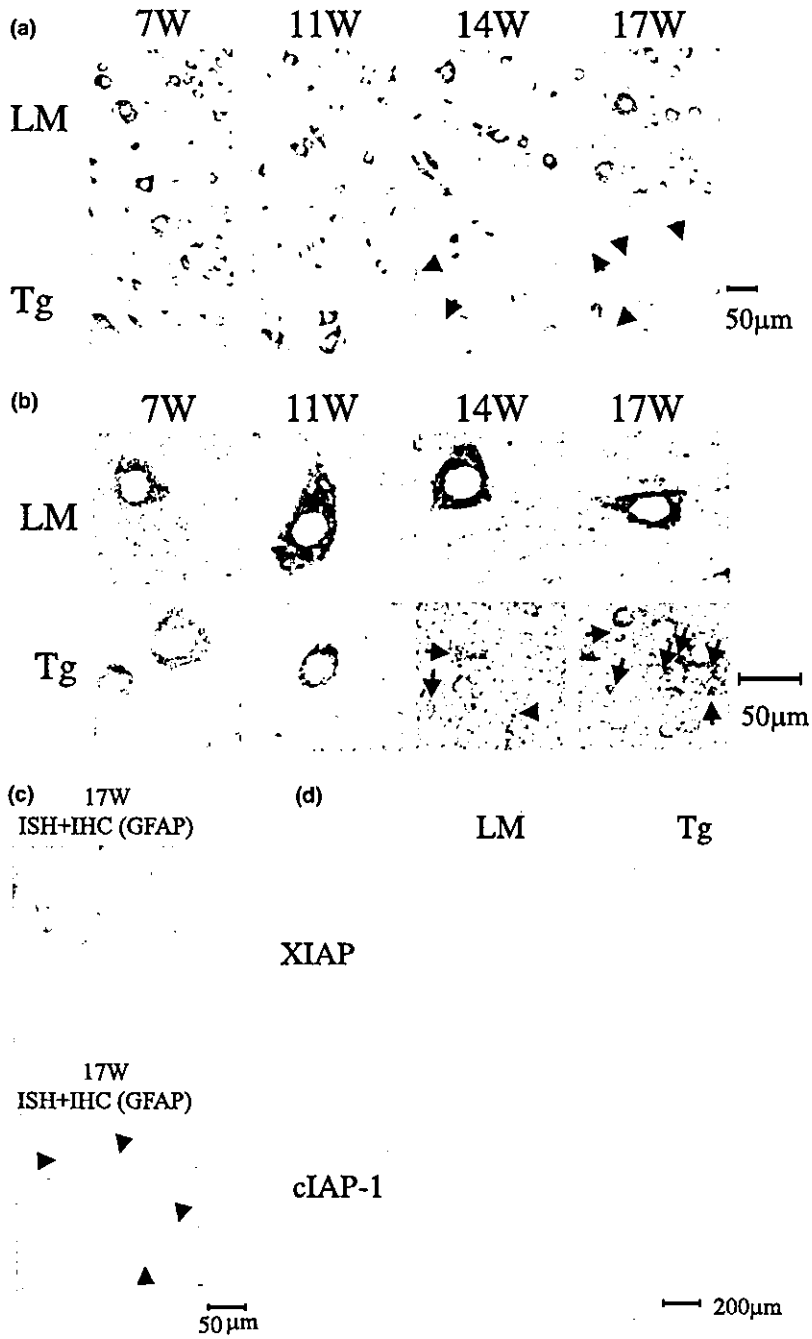

Fig. 3 *In situ* hybridization (ISH) analysis in the G93A-SOD1 transgenic mouse (Tg) and normal littermates (LM) spinal cord at 7, 11, 14 and 17 weeks (a, b and c) and brain at 14 weeks (d). The transverse sections were hybridized with digoxigenin-labeled cRNA probes of mouse XIAP and cIAP-1. It was confirmed that no signal was detected when using sense probes. (a) The expression of XIAP is seen in both motor neurons and glial cells in the spinal cords of LM. In the spinal cords of Tg at 14 and 17 weeks, its expression is significantly decreased in a subpopulation of motor neurons whose morphological appearance is indistinguishable from normal ones (arrows). (b) The expression of cIAP-1 is also seen in motor neurons and glial cells, but mainly expressed in normal motor neurons in the spinal cords of LM. However, the expression of cIAP1 in glial cells increased as reactive gliosis occurred in the spinal cords of Tg at 14 and 17 weeks (arrows). (c) ISH followed by immunostaining of GFAP showed that the signal of cIAP1 mRNA (blue) and the staining of GFAP (pink) were merged in the spinal cords of Tg at 17 weeks (arrowheads). (d) Expressions of XIAP and cIAP1 are seen mainly in neurons of hippocampus in the brain at 14 weeks.

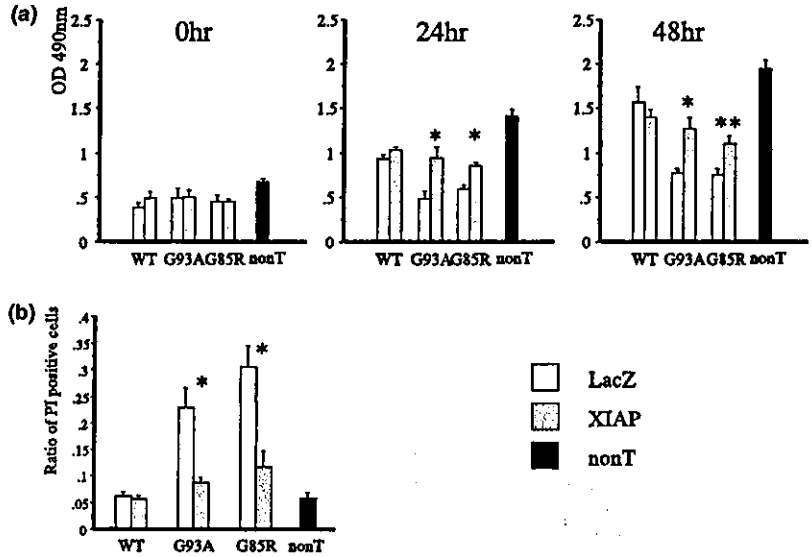

Fig. 4 (a) The rescue effect of XIAP expression in mutant SOD1 cells on MTT assay. Neuro2a cells were grown in 96 collagen-coated wells and then transfected with WT-pcDNA3.1/MycHis (WT), G93A-pcDNA3.1/MycHis (G93A) or G85R-pcDNA3.1/MycHis (G85R) and XIAP-pcDNA4/HisMax (XIAP) or pcDNA4/HisMax-LacZ (LacZ). Cells without transfection were used as a negative control (non-T). After the medium was changed, MTT assays were performed at 0, 24 and 48 h of incubation. Viability was measured as the level of absorbance (490 nm). Values are the means ± SD, $n = 3$. Statistics were carried out by one-way ANOVA. $^{*}p < 0.01$, $^{**}p < 0.001$ denotes significant difference between cells with LacZ and cells with XIAP. (b) Cell death assay using propidium iodide (PI) staining. Neuro2a cells were transfected with WT, G93A or G85R and XIAP or LacZ. The C3-EGFP vector was also transfected as a marker of transfected cells. Cells only transfected with C3-EGFP vector were used as a negative control (N). After 48 h of serum withdrawal, the ratio of PI positive cells in GFP positive cells was calculated. Values are the means ± SD, $n = 3$. Statistical tests were done using one-way ANOVA. $^{*}p < 0.001$ denotes significant difference between cells with LacZ and cells with XIAP.

(WT/LacZ) and those with WT-SOD1 and XIAP (WT/XIAP); cells with G93A-SOD1 and LacZ (G93A/LacZ) and those with G93A-SOD1 and XIAP (G93A/XIAP); or cells with G85R-SOD1 and LacZ (G85R/LacZ) and those with G85R-SOD1 and XIAP (G85R/XIAP). After 24 h of incubation, the viability of G93A/XIAP was significantly higher than that of G93A/LacZ, and the viability of G85R/XIAP also showed a higher level than that of G85R/LacZ, but there was no difference among cells with WT. At 48 h the viability of G93A/XIAP and G85R/XIAP was also increased compared with G93A/LacZ and G85R/LacZ, respectively (Fig. 4a).

Cell death was assessed using PI staining after 48 h of serum deprivation. Co-expression of XIAP reduced the number of PI-positive cells in both G93A- and G85R-SOD1-expressing cells to approximately half of those coexpressing LacZ (Fig. 4b).

BIR1-2 domain protects against cell death in neuro2a cells expressing mutant SOD1, while BIR3-RING does not

We established two deletional constructs of XIAP, BIR1-2 (residues 1–241) and BIR3-RING (residues 242–496), to examine which domain of XIAP is responsible for the inhibition of cell death in mutant SOD1 harboring cells. The MTT assay revealed that after 24 and 48 h of incubation, the viability of cells with BIR1-2 and G93A-SOD1 or BIR1-2 and G85R-SOD1 was significantly higher than that of cells with LacZ and G93A-SOD1 or LacZ and G85R-SOD1. However, BIR3-RING did not show any significant difference in cells with mutant SOD1 at any time in culture (Fig. 5a).

Cell death assay with PI staining also indicated that the cell death ratio of neuro2a cells with BIR1-2 and G93A-SOD1 or BIR1-2 and G85R-SOD1 was significantly lower than that of cells with LacZ and G93A-SOD1 or LacZ and G85R-SOD1. In contrast, BIR3-RING failed to prevent cell death in neuro2a with mutant SOD1 (Fig. 5b).

Inhibition of caspase-3 activation by XIAP in neuro2a cells expressing mutant SOD1

We detected the activated form of caspase-3 in neuro2a cells with G93A/LacZ and G85R/LacZ followed by serum deprivation and oxidative stress (H_2O_2; 100 μM), whereas a much less activated caspase-3 was found in cells with wild type SOD1 or in cells without transfection. When XIAP was coexpressed, the activated form of caspase-3 was markedly diminished in the cells expressing mutant SOD1 followed by serum deprivation and oxidative stress (Fig. 6).

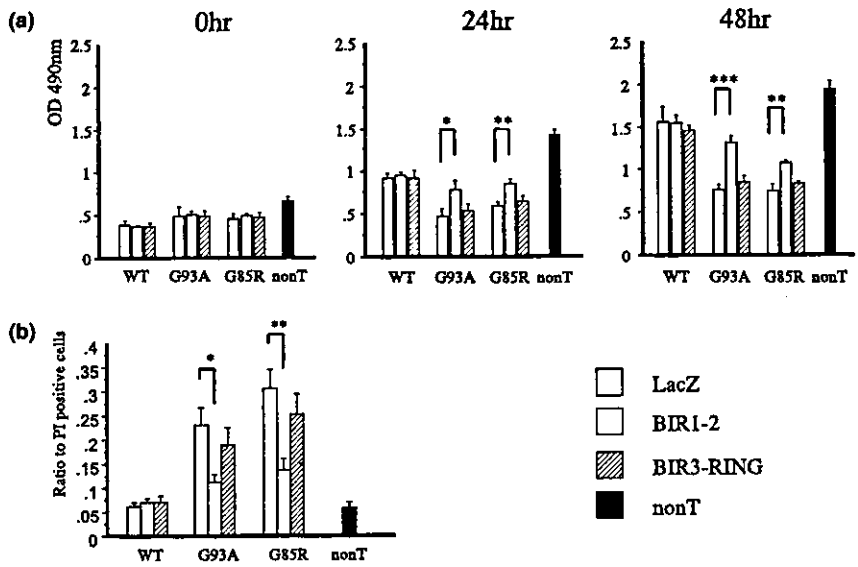

Fig. 5 Effects of deletional constructs on MTT assay. The N terminal fragment, BIR1-2 (residues 1–241), and the C terminal fragment, BIR3-RING (residues 242–496), were inserted in pcDNA4/His-Max vectors, and then cotransfected with WT-pcDNA3.1/MycHis (WT), G93A-pcDNA3.1/MycHis (G93A) or G85R-pcDNA3.1/MycHis (G85R) as in Fig. 3 (a). Cells without transfection were used as a negative control (non-T). Values are the means ± SD, $n = 3$. Statistical tests were done using one-way ANOVA. $^{*}p < 0.05$, $^{**}p < 0.01$ and $^{***}p < 0.001$ denote significant difference between cells with LacZ and cells with XIAP. (b) Effects of deletional constructs for cell death by PI staining. Neuro2a cells were transfected with WT, G93A or G85R and BIR1-2, BIR3-RING or LacZ and C3-EGFP-Mock as in Fig. 3 (b). Cells only transfected with C3-EGFP vector were used as a negative control (N). Values are the means ± SD, $n = 3$. Statistical tests were done using one-way ANOVA. $^{*}p < 0.01$ and $^{**}p < 0.001$ indicate significant difference between cells with LacZ and cells with BIR1-2.

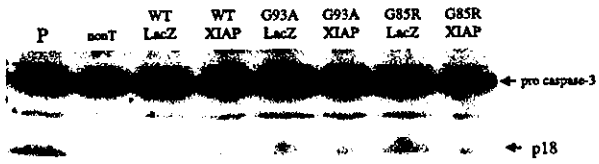

Fig. 6 Inhibition of caspase-3 activation by XIAP in mutant SOD1 neuro2a cells. Immunoblots show the active form of caspase-3 (p18) in neuro2a cells expressing WT, G93A-SOD1 or G85R-SOD1, and XIAP or LacZ. Cells were treated with 100 μM of H_2O_2 for 4 h following 48 h of serum deprivation. Ten micrograms of each sample was loaded in each lane. Cells treated with 0.01 μM of staurosporin were used as positive control (P). Non-transfected cells were loaded as negative control (non-T).

Discussion

In this study we demonstrated that the expressions of XIAP mRNA and protein were markedly decreased in the spinal cord of mutant SOD1 Tg mice when symptomatic impairment occurred, whereas its expression in the unaffected region of brain was unchanged. The ISH study revealed that the expression of XIAP mRNA was diminished in subpopulations of motor neurons without correlation to morphological changes such as vacuolation or shrinkage of motor neurons, indicating that the decrease in XIAP was due to the decline of XIAP expression in subpopulations of surviving motor neurons. The mechanism regulating XIAP mRNA expression remains unknown. However, strict regulation of the XIAP protein level has been shown, and some molecules, such as Smac/DIABLO, NAF1 or HtrA2 can inactivate XIAP protein by disrupting its caspase-binding domain (Verhagen *et al.* 2000; Liston *et al.* 2001; Suzuki *et al.* 2001b). XIAP protein can be cleaved by caspases at a point between BIR2 and BIR3, and the XIAP protein itself is autoubiquitinated (Deveraux *et al.* 1999; Yang *et al.* 2000). It was reported that XIAP was cleaved in the spinal cord of G93A-SOD1 Tg mice at the end stage (Guégan *et al.* 2001). We detected a decrease in XIAP protein but did not detect the cleaved fragment of XIAP in G93A-SOD1 Tg mice at 14 weeks, the early symptomatic stage. The discrepancy could be due to the difference of disease stage. It is possible that the expression of XIAP is depleted when symptoms occurred, and then cleaved when caspases are prominently activated at the advanced end stage.

We also showed that the expression of another IAP family, cIAP-1, was increased in the spinal cord of symptomatic G93A-SOD1 Tg mice. The ISH study followed by immunostaining for GFAP revealed that this cIAP-1 mRNA up-regulation was seen in reactive astrocytes in the spinal cord of G93A-SOD1 Tg mice. Interestingly, in XIAP knockout mice, the levels of cIAP-1 and cIAP-2 proteins were increased, though the mice showed no obvious symptoms (Harlin *et al.* 2001). This observation suggests that cIAP-1

and cIAP-2 compensate for the loss of inhibitory activity for apoptosis due to the loss of XIAP. Furthermore, considerable data support the view that glial cells, particularly astrocytes, take part in motor neuron death in the mutant SOD1 Tg mouse (Bruijn *et al.* 1997; Gong *et al.* 2000; Pramatarova *et al.* 2001). Glial cell up-regulation of cIAP-1 in our study may thus reflect some compensatory role of cIAP-1 for the decreased XIAP in the motor neurons of Tg mice, although these events occur in different cell lineages.

It has been demonstrated that IAP family proteins, including XIAP, can compromise cell death in various neuronal disease models. For example, the overexpression of XIAP can attenuate rat ischemia-induced cellular and behavioral deficits (Xu *et al.* 1999), and adenovirus-mediated overexpression of XIAP inhibits of dopaminergic neuron death in the substantia nigra induced by MPTP (Eberhardt *et al.* 2000). In addition, apoptotic cell death in cerebellar granule neurons (Simons *et al.* 1999) and glioma cells (Wagenknecht *et al.* 2000) was attenuated by XIAP. Furthermore, neuronal apoptosis inhibitory protein, cIAP-1 and cIAP-2, can delay the death of motoneurons after axotomy (Parrelet *et al.* 2000).

In the present study, we clearly demonstrated that the overexpression of XIAP rescued a neuro2a cell line expressing G93A-SOD1 and G85R-SOD1 from cell death. By deletional mutant analysis, we showed that the N-terminal fragment, BIR1-2, was essential for the inhibition of cell death in neuro2a cells with mutant SOD1, whereas the C-terminal fragment, BIR3-RING, was not. It has been demonstrated that the BIR1-2 domain is sufficient and specific for the inhibition of caspase-3 and caspase-7, while BIR3-RING is sufficient and specific for caspase-9 inhibition (Deveraux *et al.* 1999). We also demonstrated that the activation of caspase-3 was compromised by the overexpression of XIAP in neuro2a cells expressing mutant SOD1. This evidence strongly suggests that increased caspase-3 activity, under a low level of XIAP expression, is a toxic executioner in the death of mutant SOD1-associated motor neurons. Although Guégan *et al.* reported that the activation of caspase-9 was also involved in the spinal cords of mutant SOD1 Tg mice (Guégan *et al.* 2001), we failed to show such activation in mutant SOD1-mediated cell death of neuro2a cells (data not shown). This discrepancy could be related to culture conditions, such as serum deprivation or oxidative stress, which is necessary for culture cells with mutant SOD1 to induce proper activation of caspase cascade.

This study strongly suggests that XIAP is a pivotal molecule for motor neuron death in the mutant SOD1 Tg mouse, and probably in familial ALS associated with mutant SOD1. Further research, including the development of double transgenic mice, will be necessary to provide an evidence that XIAP can inhibit or delay the onset and progression of mutant SOD1-associated ALS.

Acknowledgements

We wish to thank Dr Naoyuki Taniguchi (Department of Biochemistry, Osaka University Medical School) for the human G93A- and G85R-SOD1 constructs. This work was supported by a grant for the Center of Excellence (COE) from the Ministry of Education, Culture, Sports, Science and Technology of Japan.

References

Bruijn L. I., Becher M. W., Lee M. K., Anderson K. L., Jenkins N. A., Copeland N. G., Sisodia S. S., Rothstein J. D., Borchelt D. R., Price D. L. and Cleaveland D. W. (1997) ALS-linked SOD1 mutant G85R mediates damage to astrocytes and promotes rapidly progressive disease with SOD1-containing inclusions. *Neuron* **18**, 327–338.

Deveraux Q. L., Takahashi R., Salvesen G. S. and Reed J. C. (1997) X-linked IAP is a direct inhibitor of cell-death proteases. *Nature* **388**, 300–304.

Deveraux Q. L., Roy N., Stennicke H., Arsdale T., Zhou Q., Srinivasula S., Alnemri E., Salvesen S. and Reed J. (1998) IAPs block apoptotic events induced by caspase-8 and cytochrome *c* by direct inhibition of distinct caspases. *EMBO J.* **17**, 2215–2213.

Deveraux Q. L., Leo E., Stennicke H., Welsh K., Salvesen G. S. and Reed J. (1999) Cleavage of human inhibitor of apoptosis protein XIAP results in fragments with distinct specificities for caspases. *EMBO J.* **18**, 5242–5251.

Doyu M., Sawada K., Mitsuma N., Niwa J., Yoshimoto M., Fujii Y., Sobue G. and Kato K. (2001) Gene expression profile in Alzheimer's brain screened by molecular indexing. *Mol. Brain Res.* **87**, 1–11.

Eberhardt O., Coelln R. V., Kugler S., Lindenau J., Rathke-Hartlieb S., Gerhardt E., Haid S., Isenmann S., Gravel C., Srinivasan A., Bahr M., Weller M., Dichgans J. and Schulz J. B. (2000) Protection by synergistic effects of adenovirus-mediated X-chromosomal-linked inhibitor of apoptosis and glial cell line-derived neurotrophic factor gene transfer in the 1-methyl-4-phenyl-1,2,3,6-tetrahydropyridine model of Parkinson's disease. *J. Neurosci.* **20**, 9126–9134.

Ghadge G. D., Lee J. P., Bindokas V. P., Jordan J., Ma L., Miller R. J. and Ross R. P. (1997) Mutant superoxide dismutase-1-linked familial amyotrophic lateral sclerosis: Molecular mechanism of neuronal death and protection. *J. Neurosci.* **17**, 8756–8766.

Gong Y. H., Parsadanian A. S., Andreeva A., Snider W. D. and Elliott J. L. (2000) Restricted expression of G86R Cu/Zn superoxide dismutase in astrocytes results in astrocytosis but does not cause motoneuron degeneration. *J. Neurosci.* **20**, 660–665.

Guégan C., Vila M., Rosoklija G., Hays A. P. and Przedborski S. (2001) Recruitment of the mitochondrial-dependent apoptotic pathway in amyotrophic lateral sclerosis. *J. Neurosci.* **21**, 6569–6576.

Gurney M. E., Pu H., Chiu A. Y., Dal Canto M. C., Polchow C. Y., Alexander D. D., Caliendo J., Hentati A., Kwon Y. W., Deng H. X., Chen W., Zhai P., Sufit R. L. and Siddique T. (1994) Motor neuron degeneration in mice that express a human Cu,Zn superoxide dismutase mutation. *Science* **264**, 1772–1775.

Harlin H., Reffey S. B., Duckett C. S., Lindsten T. and Thompson C. B. (2001) Characterization of XIAP-deficient mice. *Mol. Cell. Biol.* **21**, 3602–3608.

Ishigaki S., Niwa J., Yoshihara T., Mitsuma N., Doyu M. and Sobue G. (2000) Two novel genes, human neugrin and mouse m-neugrin, are upregulated with neuronal differentiation in neuroblastoma cells. *Biochem. Biophys. Res. Commun.* **279**, 526–533.

Kostic V., Jackson-Lewis V., de Bilbao F., Dubois-Dauphin M. and Przedborski S. (1997) Bcl-2: prolonging life in a transgenic mouse

model of familial amyotrophic lateral sclerosis. *Science* **277**, 559–562.

Lee M., Hyun D.-H., Hailliwell B. and Jenner P. (2001) Effect of overexpression of wild-type and mutant Cu/Zn-superoxide dismutases on oxidative stress and cell death induced by hydrogen peroxide, 4-hydroxynonenal or serum deprivation: potentiation of injury by ALS-related mutant superoxide dismutases and protection by Bcl-2. *J. Neurochem.* **78**, 209–220.

Li M., Ona V. O., Guégan C., Chen M., Jackson-Lewis V., Andrews L. J., Olzewski A. J., Stieg P. E., Lee J. P., Przedborski S. and Frielander R. M. (2000) Functional role of caspase-1 and caspase-3 in an ALS transgenic mouse model. *Science* **288**, 335–339.

Liston P., Fong W. G., Kelly N. L., Toji S., Miyazaki T., Conte D., Tamai K., Craig C. G., McBurney M. W. and Korneluk R. G. (2001) Identification of XAF1 as an antagonist of XIAP anti-caspase activity. *Nat. Cell Biol.* **3**, 128–133.

Niwa J., Ishigaki S., Doyu M., Suzuki T., Tanaka K. and Sobue G. (2001) A novel centrosomal ring-finger protein, dorfin, mediates ubiquitin ligase activity. *Biochem. Biophys. Res. Commun.* **281**, 706–713.

Parrelet D., Ferri A., MacKenzie A. E., Smith G. M., Korneluk R. G., Liston P., Sagot Y., Terrado J., Monnier D. and Kato A. C. (2000) IAP family proteins delay motoneuron cell death *in vivo*. *Eur. J. Neurosci.* **12**, 2059–2067.

Passinelli P., Borchelt D. R., Houseweart M. K., Cleaveland D. W. and Brown R. H. Jr (1998) Caspase-1 is activated in neuronal cells and tissue with amyotrophic lateral sclerosis-associated mutation in copper-zinc superoxide dismutase. *Proc. Natl Acad. Sci. USA* **95**, 15763–15768.

Passinelli P., Houseweart M. K., Brown R. H. Jr and Cleaveland D. W. (2000) Caspase-1 and -3 are sequentially activated in motor neuron death in Cu,Zn superoxide dismutase-mediated familial amyotrophic lateral sclerosis. *Proc. Natl Acad. Sci. USA* **97**, 13901–13906.

Pramatarova A., Laganière J., Roussel J., Brisebois K. and Rouleau G. A. (2001) Neuron-specific expression of mutant superoxide dismutase 1 in transgenic mice does not lead to motor impairment. *J. Neurosci.* **15**, 3369–3374.

Rosen D. R., Siddique T., Patterson D., Figlewicz D. A., Sapp P., Hentati A., Donaldson D., Goto J., O'Regan J. P., Deng H. X. *et al.* (1993) Mutations in Cu/Zn superoxide dismutase gene are associated with familial amyotrophic lateral sclerosis. *Nature* **362**, 59–62.

Roy N., Deveraux Q. L., Takahashi R., Salvesen G. S. and Reed J. C. (1997) The cIAP-1 and cIAP-2 proteins are direct inhibitors of specific caspases. *EMBO J.* **16**, 6914–6925.

Simons M., Beinroth S., Gleichmann M., Liston P., Korneluk R. G., MacKenzie A. E., Bähr M., Klockgether T., Robertoson G. S., Weller M. and Schulz J. B. (1999) Adenovirus-mediated gene transfer of inhibitory apoptosis protein delays apoptosis in cerebellar granule neurons. *J. Neurochem.* **72**, 292–301.

Suzuki Y., Nakabayashi Y. and Takahashi R. (2001a) Ubiquitin-protein ligase activity of X-linked inhibitor of apoptosis protein promotes proteasomal degradation of caspase-3 and enhances its anti-apoptotic effect in Fas-induced cell death. *Proc. Natl Acad. Sci. USA* **98**, 8662–8667.

Suzuki Y., Imai Y., Nakayama H., Takahashi K., Takio K. and Takahashi R. (2001b) A serin protease, HtrA2, is released from the mitochondria and interacts with XIAP, including cell death. *Mol. Cell* **8**, 613–621.

Takahashi R., Deveraux Q., Tamm I., Welsh K., Assa-Munt N., Salvesen G. S. and Reed J. C. (1998) A single BIR domain of XIAP sufficient for inhibiting caspases. *J. Biol. Chem.* **273**, 7787–7790.

Verhagen A. M., Ekert P. G., Pakusch M., Silke J., Connolly L. M., Reid G. E., Moritz R. L., Simpson R. J. and Vaux D. L. (2000) Identification of DIABLO, a mammalian protein that promotes apoptosis by binding to and antagonizing IAP proteins. *Cell* **102**, 43–53.

Vukosavic S., Stefanis L., Jackson-Lewis V., Guégan C., Romero N., Chen C., Dubois-Dauphin M. and Przedborski S. (2000) Delaying caspase activation by Bcl-2: a clue to disease retardation in a transgenic mouse model of amyotrophic lateral sclerosis. *J. Neurosci.* **20**, 9119–9125.

Wagenknecht B., Hermisson M., Groscurth P., Liston P., Krammer P. H. and Weller M. (2000) Proteasome inhibitor-induced apoptosis of glioma cells involves the processing of multiple caspases and cytochrome c release. *J. Neurochem.* **75**, 2288–2297.

Xu D., Bureau Y., McIntyre D. C., Nicholson D. W., Liston P., Zhu Y., Fong W. G., Crocker S. J., Korneluk R. G. and Robertson G. S. (1999) Attenuation of ischemia-induced cellular and behavioral deficits by X chromosome-linked inhibitor of apoptosis protein overexpression in the rat hippocampus. *J. Neurosci.* **19**, 5026–5033.

Yamamoto M., Li M., Mitsuma N., Ito S., Kato M., Takahashi M. and Sobue G. (2001) Preserved phosphorylation of RET receptor protein in spinal motor neurons of patients with amyotrophic lateral sclerosis: an immunohistochemical study by a phosphorylation-specific antibody at tyrosine 1062. *Brain Res.* **912**, 89–94.

Yang Y., Fang S., Jenson J. P., Weissman A. M. and Ashwell J. D. (2000) Ubiquitin-protein ligase activity of IAPs and their degradation in proteasomes in response to apoptotic stimuli. *Science* **288**, 874–877.

Yoshihara T., Ishigaki S., Yamamoto M., Liang Y., Niwa J., Takeuchi H., Doyu M. and Sobue G. (2002) Differential expression of inflammation- and apoptosis-related genes in spinal cords of a mutant SOD1 transgenic mouse model of familial amyotrophic lateral sclerosis. *J. Neurochem.* **80**, 158–167.

THE JOURNAL OF BIOLOGICAL CHEMISTRY
Vol. 277, No. 39, Issue of September 27, pp. 36793–36798, 2002
Printed in U.S.A.

Dorfin Ubiquitylates Mutant SOD1 and Prevents Mutant SOD1-mediated Neurotoxicity*

Received for publication, July 2, 2002
Published, JBC Papers in Press, July 26, 2002, DOI 10.1074/jbc.M206559200

Jun-ichi Niwa‡§, Shinsuke Ishigaki‡, Nozomi Hishikawa‡, Masahiko Yamamoto‡, Manabu Doyu‡, Shigeo Murata¶, Keiji Tanaka¶, Naoyuki Taniguchi‖, and Gen Sobue‡**

From the ‡Department of Neurology, Nagoya University Graduate School of Medicine, Showa-ku, Nagoya 466-8550, Japan, the ¶Department of Molecular Oncology, Tokyo Metropolitan Institute of Medical Science, Bunkyo-ku, Tokyo 113-8613, Japan, and the ‖Department of Biochemistry, Osaka University Graduate School of Medicine, Suita, Osaka 565-0871, Japan

Amyotrophic lateral sclerosis (ALS) is a progressive paralytic disorder resulting from the degeneration of motor neurons in the cerebral cortex, brainstem, and spinal cord. The cytopathological hallmark in the remaining motor neurons of ALS is the presence of ubiquitylated inclusions consisting of insoluble protein aggregates. In this paper we report that Dorfin, a RING finger-type E3 ubiquitin ligase, is predominantly localized in the inclusion bodies of familial ALS with a copper/zinc superoxide dismutase (SOD1) mutation as well as sporadic ALS. Dorfin physically bound and ubiquitylated various SOD1 mutants derived from familial ALS patients and enhanced their degradation, but it had no effect on the stability of the wild-type SOD1. The overexpression of Dorfin protected against the toxic effects of mutant SOD1 on neural cells and reduced SOD1 inclusions. Our results indicate that Dorfin protects neurons by recognizing and then ubiquitylating mutant SOD1 proteins followed by targeting them for proteasomal degradation.

Amyotrophic lateral sclerosis (ALS)[1] is a neurodegenerative disease characterized by the loss of motor neurons in the cerebral cortex, brain stem, and spinal cord (1, 2). Although most patients with ALS are sporadic cases, 5–10% of ALS patients show a familial trait, and in 10–20% of these patients this trait is associated with mutations in the *SOD1* gene (3). Although many scenarios for understanding ALS pathogenesis have been proposed (4–6), to date the exact mechanisms causing the disease are still unknown. In considering the pathogenesis of ALS, it is important that the inclusion bodies, which consist of aggregated, ubiquitylated proteins surrounded by disorganized filaments, are frequently seen in the surviving motor neurons in both sporadic and familial ALS (7–12). Interestingly, SOD1 is reported to be the major component of the neuronal hyaline inclusion (NHI) of familial ALS associated with SOD1 mutation (13). In addition, the NHI in the motor neurons of familial ALS is commonly stained with anti-ubiquitin (Ub)-antibody, but it remains uncertain whether SOD1 itself is ubiquitylated with respect to the inclusion body formation. To clarify the mechanisms underlying the inclusion body formation and consequent motor neuron degeneration in ALS, it is important to know how SOD1 and/or other protein component(s) are ubiquitylated.

Dorfin is a gene product we cloned from the anterior horn tissues of the human spinal cord (14). Dorfin contains two RING finger motifs and an in-between RING finger (IBR) domain at the N terminus (14). The RING finger/IBR motif was identified in several protein sequences through a data base search (15). It was reported that HHARI (human homologue of ariadne) and H7-AP1 (UbcH7-associated protein), which are both RING finger/IBR motif-containing proteins, interact with the ubiquitin-conjugating enzyme (E2) UbcH7 through the RING finger/IBR motif and that a distinct subclass of RING finger/IBR motif-containing proteins represents a new family of proteins that specifically interact with distinct E2 enzymes (16, 17). Parkin, a gene product responsible for one of the most common forms of the familial Parkinson's disease (PD) (18), has a RING finger/IBR motif, binds with UbcH7 and UbcH8, and has ubiquitin-protein ligase (E3) activities (19–21). Several proteins with RING finger motifs have been characterized as E3 ubiquitin ligases (22–24). In RING-type E3s, the RING finger motifs function as recruiting motifs for specific E2s (25–28). These facts suggest that RING finger/IBR family proteins are new members of the RING-type E3 family. We found that Dorfin interacts with UbcH7 or UbcH8 through the RING finger/IBR domain and mediates E3 activity (14).

We reported previously (14) that Dorfin is mainly localized in the centrosomal region and forms an aggresome-like structure. Aggresomes are pericentriolar cytoplasmic inclusions containing misfolded ubiquitylated proteins, which appear when the cell fails to further degrade misfolded proteins (29). In addition, cultured cells expressing mutant SOD1 have been demonstrated to form an aggresome-like structure (30). Based on this background, we postulated that Dorfin could be critically important in the formation of ubiquitylated inclusion bodies in ALS. We show here that Dorfin is localized in the inclusion bodies found in the motor neurons of familial ALS with a SOD1 mutation as well as sporadic ALS and mutant SOD1-trans-

* This work was supported in part by a Center of Excellence (COE) grant from the Ministry of Education, Culture, Sports, Science and Technology and grants from the Ministry of Health, Labor and Welfare of Japan. The costs of publication of this article were defrayed in part by the payment of page charges. This article must therefore be hereby marked "*advertisement*" in accordance with 18 U.S.C. Section 1734 solely to indicate this fact.

§ Research fellow of the Japan Society for the Promotion of Science for Young Scientists.

** To whom correspondence should be addressed: Department of Neurology, Nagoya University Graduate School of Medicine, 65 Tsurumai-cho Showa-ku, Nagoya 466-8550, Japan. Tel.: 81-52-744-2385; Fax: 81-52-744-2384; E-mail: sobueg@med.nagoya-u.ac.jp.

[1] The abbreviations used are: ALS, amyotrophic lateral sclerosis; SOD1, copper/zinc superoxide dismutase; NHI, neuronal hyaline inclusion; Ub, ubiquitin; IBR, in-between RING finger; HEK293, human embryonic kidney 293; E2, ubiquitin-conjugating enzyme; E3, ubiquitin-protein ligase; IP, immunopurified; PI, propidium iodide; GFP, green fluorescent protein; MTT, 3-(4,5-dimethylthiazol-2yl)-2,5-diphenyltetrazolium bromide; PD, Parkinson's disease; CHIP, carboxyl terminus of Hsc70-interacting protein; Hsp, heat shock protein.